Copy No. 1

RM SA9H22

NACA

RESEARCH MEMORANDUM

for the

Air Materiel Command, U. S. Air Force

WIND-TUNNEL TESTS OF A 0.16-SCALE MODEL OF THE DOUGLAS MX-656 AIRPLANE AT HIGH SUBSONIC SPEEDS. II -- WING AND FUSELAGE PRESSURE DISTRIBUTION

By Joseph W. Cleary and Jack A. Mellenthin

Ames Aeronautical Laboratory
Moffett Field, Calif.

NATIONAL ADVISORY COMMITTEE
FOR AERONAUTICS

WASHINGTON

August 22, 1949

NACA RM SA9H22

NATIONAL ADVISORY COMMITTEE FOR AERONAUTICS

RESEARCH MEMORANDUM

for the

Air Materiel Command, U. S. Air Force

WIND-TUNNEL TESTS OF A 0.16-SCALE MODEL OF THE DOUGLAS MX-656 AIRPLANE AT HIGH SUBSONIC SPEEDS. II - WING AND FUSELAGE PRESSURE DISTRIBUTION

By Joseph W. Cleary and Jack A. Mellenthin

SUMMARY

Measurements of wing and fuselage pressure distributions were made at low and high subsonic Mach numbers on a 0.16-scale model of the projected MX-656 research airplane. The MX-656 is a supersonic design utilizing a low-aspect-ratio wing and tail.

Pressure-distribution measurements indicated that, although the critical Mach number of the wing was approximately 0.81 at 0° angle of attack, compressibility effects were of little significance below a Mach number of at least 0.90. The principal effect of compressibility was an increase in the pressure gradient over the after 30 percent of the wing chord, causing a tendency for the flow to separate.

At 0.40 Mach number, the wing stalled abruptly at approximately 12° angle of attack. The wing-pressure distribution showed this stall was a result of complete separation of the flow from the upper surface of the wing. Deflecting the leading-edge flaps delayed the stall to a higher angle of attack with some increase in the maximum section normal force.

INTRODUCTION

Measurements of wing and fuselage pressure distributions were made on a 0.16-scale model of the Douglas MX-656 airplane in conjunction with high-speed lateral- and longitudinal-stability tests (reference 1) as it was desired to calculate the chord and span

loading, to estimate the critical Mach number of the wing and fuselage combination, and to furnish aerodynamic data of general interest on this supersonic design.

The tests were conducted in the Ames 16-foot high-speed wind tunnel and were made at the request of the U. S. Air Force. The tests extended over a Mach number range from 0.40 to 0.925.

COEFFICIENTS AND SYMBOLS

The following definitions apply to the coefficients and symbols used in this report:

c_n section normal-force coefficient $\left(\frac{\text{section normal force}}{qS}\right)$

P pressure coefficient $\left(\frac{p_l - p_s}{q}\right)$

P_{cr} critical pressure coefficient (the pressure coefficient at which the local velocity became sonic)

b wing span, feet

S wing area, square feet

c wing chord, feet

c_{av} average wing chord $\left(\frac{S}{b}\right)$, feet

$\bar{c}$ mean aerodynamic chord of the wing $\left(\frac{\int_0^{b/2} c^2\, dy}{\int_0^{b/2} c\, dy}\right)$, feet

L.E. leading edge

M free-stream Mach number

M_{cr} critical Mach number (the free-stream Mach number for which sonic flow first occurred on the model at the station or point being considered)

p_l local static pressure, pounds per square foot

p_s free-stream static pressure, pounds per square foot

q free-stream dynamic pressure $\left(\frac{1}{2}\rho V^2\right)$, pounds per square foot

v local velocity, feet per second

V free-stream velocity, feet per second

y perpendicular distance along the wing semispan from the plane of symmetry, feet

α angle of attack of the fuselage reference line corrected for the effects of the tunnel walls, degrees

α_u angle of attack of the fuselage reference line uncorrected for the effects of the tunnel walls, degrees

δ_{lf} leading-edge flap-deflection, positive downward, degrees

ρ mass density of the free stream, slugs per cubic foot

ψ_u angle of yaw of the fuselage reference line uncorrected for the effects of the tunnel walls, degrees

MODEL AND APPARATUS

Figure 1 shows the location of the pressure-orifice stations on the wing and fuselage of the model. Pressure-orifice stations on the left wing were 9.02 and 16.56 inches from the plane of symmetry while those on the right wing were 12.16 and 19.20 inches from the same reference plane. The orifices on the fuselage were in longitudinal rows as shown in the sketch. A total-pressure rake was installed on the fuselage at station 43.20 inches to measure the thickness of the boundary layer at a location that corresponded to the entrance of the left boundary-layer-bleed scoop. Figures 2, 3, and 4 are photographs of the model and of the installation of the boundary-layer rake.

The 0.16-scale model had an aspect ratio of 3.01 and a wing taper ratio of 0.4. The 75-percent-chord line of the wing was perpendicular to the plane of symmetry. The wing had a symmetrical hexagonal section 4.5 percent thick with rounded corners at 30- and 70-percent chord and sharp leading and trailing edges. Figure 1 shows a typical section through the wing. A detailed description of the model and a table of dimensions are given in reference 1.

The model for all pressure measurements consisted of the wing, the tail, and the fuselage with the tail boom. The canopy, air scoops, and nose fins were omitted.

The model was supported on a sting that carried the pressure leads from the model to mercury-in-glass manometers. Pressure-distribution measurements were made in pitch at 0° angle of yaw and,

in yaw, at approximately 6.2° angle of attack. With the model mounted so that wing span was vertical, the angle of yaw was varied with the mechanism normally used to vary the angle of attack. (See fig. 3.) The angles of attack and of yaw of the model were measured visually with a protractor mounted outside the tunnel test section.

REDUCTION OF DATA

The wind-tunnel-wall and constriction corrections are given in reference 1.

Section normal-force data were derived by mechanical integration of pressure-distribution plots. The section loading coefficients were computed by multiplying the section normal-force coefficients by the ratio of the section chord to the average wing chord.

RESULTS AND DISCUSSION

Characteristics in Pitch

Wing pressure distribution.- The distribution of pressure over the wing of the model with the leading-edge flaps undeflected is shown in figure 5. As the angle of attack was increased, at 0.40 Mach number, the minimum pressure coefficient near the leading edge increased in absolute value up to an angle of attack of approximately 3° to 6°. Further increase in angle of attack extended the region of approximately uniform minimum pressure on the upper surface until at 12° it covered from 25 to 60 percent of the chord. Between 12° and 15° angle of attack, the flow over the whole upper surface separated and remained separated at the higher angles of attack. The changes in pressure distribution between 6° and 12° angle of attack represent a rearward shift of the center of pressure and appear as a stable variation of the tail-off pitching moment in the data of reference 1.

The effects of compressibility do not appear significant below a Mach number of approximately 0.90. At Mach numbers of 0.90 and 0.925, for a given angle of attack, the pressure gradients were steeper over the after 30 percent of the chord than at the lower Mach numbers. The flow also had a tendency toward earlier separation, a factor which might cause some loss in aileron effectiveness at the higher Mach numbers.

Deflecting the leading-edge flaps 10° and 30° (figs. 6 and 7, respectively) created a region of minimum pressure along the flap hinge line that shifted to the leading edge at the higher angles of

attack. At the higher Mach numbers and leading-edge-flap angles the flow had a tendency to separate on the upper surface behind the flap hinge line.

Fuselage pressure distribution.- Figure 8 presents the distribution of pressure over the fuselage. The relatively large negative pressures that occurred in the region of the wing are attributed to the combination of the flow fields of the wing and fuselage. The absolute value of the negative pressure coefficient on the fuselage was less than that on the wing for any given angle of attack. The separation of flow that occurred over the wing upper surface for angles of attack greater than 12° did not extend over the center of the fuselage in the region of the wing.

Critical Mach number of wing and fuselage.- The variation of critical Mach number of the wing with angle of attack is presented in figure 9 for leading-edge-flap angles of 0° and 30°. With an angle of attack of 0° and a leading-edge-flap angle of 0°, sonic flow first occurred at wing station 16.56 inches at a Mach number of 0.81. The lowest critical Mach number measured with the flaps undeflected was 0.625 at 7° angle of attack at wing station 9.02 inches.

Deflecting the leading-edge flaps 30° lowered the critical Mach number of the wing throughout the usable angle-of-attack range (fig. 9).

The variation of critical Mach number of the fuselage with angle of attack is presented in figure 10. At 0° angle of attack, the lowest critical Mach number measured on the fuselage was 0.89 on the upper row of fuselage orifices. For angles of attack between 3° and 17.5°, the lowest critical Mach number was measured on the right row of fuselage orifices.

Wing section normal-force and section loading characteristics.- Figure 11 presents the variation of section normal force with angle of attack for leading-edge-flap angles of 0° and 30°. The normal-force characteristics are in agreement with the lift characteristics presented in reference 1. Any spanwise variation of the stalling angle was difficult to detect because of the limited data in the region of the stall. The data indicate that the stall probably occurred almost simultaneously at all stations at 0.40 Mach number.

Deflecting the leading-edge flaps 30° delayed the stall and increased the section normal force at the stall almost 50 percent.

The variation of the section loading coefficient along the span for the wing outboard of station 9.02 inches is given in figures 12 and 13 for leading-edge-flap angles of 0° and 30°, respectively.

Boundary layer at fuselage station 43.2 inches.- Measurements were made to determine the thickness of the boundary layer at the entrance to the left boundary-layer-bleed scoop. (See figs. 1 and 4.) The velocity ratios in the boundary layer are shown in figure 14. The boundary-layer thickness was of the order of 0.4 inch at all Mach numbers of the test, and the thickness increased slightly with angle of attack.

Characteristics in Yaw

Wing and fuselage pressure distribution.- Figures 15 and 16 show the pressure distribution over the wing and fuselage, respectively, for several angles of yaw and an angle of attack of approximately 6.2°.

At 0° yaw and approximately 6.2° angle of attack, higher minimum pressures were observed at the leading edge (primarily station 12.16 inches) when the model was mounted with the wing span vertical for the yaw tests (fig. 3) than with the model upright for the pitch tests. A contributing factor may have been that, with the model mounted for yaw tests, the wing plane was much nearer to one of the tunnel walls than for tests with the model in the normal attitude. This was due to the fact that the tunnel is but 12 feet wide and the model was not on the tunnel center line.

Boundary layer at fuselage station 43.2 inches.- The velocity ratio in the boundary layer at a position corresponding to the entrance to the left boundary-layer-bleed scoop with the model yawed is presented in figure 17. The boundary-layer thickness appeared to decrease with increasing angle of yaw and there was an increase in energy loss at a distance from the surface for high angles of yaw.

CONCLUDING REMARKS

Wing and fuselage pressure-distribution measurements on a 0.16-scale model of the proposed Douglas MX-656 research airplane indicated that, although the critical Mach number was 0.81 at 0° angle of attack, no serious compressibility effects occurred to the flow over the model below a Mach number of 0.90. The principal Mach number effect was to increase the pressure gradient over the after 30 percent of the wing chord, causing a tendency for the flow to separate.

At 0.40 Mach number, the wing stalled at approximately 12° angle of attack. This stall appeared, from the wing pressure

distribution, to involve complete separation of the flow from the upper surface. Deflecting the leading-edge flaps 30° delayed the stall and increased the section normal force at the stall almost 50 percent.

Ames Aeronautical Laboratory,
National Advisory Committee for Aeronautics,
Moffett Field, Calif.

REFERENCE

1. Hamilton, William T., and Cleary, Joseph W.: Wind-Tunnel Tests of a 0.16-Scale Model of the Douglas MX-656 Airplane at High Subsonic Speeds. I - Stability and Control Characteristics. NACA RM SA9D26, 1949.

FIGURE LEGENDS

Figure 1.- The location of the pressure-orifice stations on the wing and fuselage of the MX-656 model.

Figure 2.- The MX-656 model mounted in the Ames 16-foot high-speed wind tunnel for pressure-distribution tests in pitch.

Figure 3.- The MX-656 model mounted in the Ames 16-foot high-speed wind tunnel for pressure-distribution tests in yaw.

Figure 4.- The fuselage boundary-layer rake mounted on the MX-656 model.

Figure 5.- The pressure distribution over the wing of the MX-656 model. Ψ, 0°; δ_{lf}, 0°.

(a) Mach number, 0.40.

Figure 5.- Continued. (b) Mach number, 0.60.

Figure 5.- Continued. (c) Mach number, 0.80.

Figure 5.- Continued. (d) Mach number, 0.90.

Figure 5.- Concluded. (e) Mach number, 0.925.

Figure 6.- The pressure distribution over the wing of the MX-656 model Ψ, 0°; δ_{lf}, 10°.

(a) Mach number, 0.40.

Figure 6.- Continued. (b) Mach number, 0.60.

Figure 6.- Continued. (c) Mach number, 0.80.

Figure 6.- Continued. (d) Mach number, 0.90.

Figure 6.- Concluded. (e) Mach number, 0.925.

Figure 7.- The pressure distribution over the wing of the MX-656 model. Ψ, 0°; δ_{lf}, 30°.

(a) Mach number, 0.40.

Figure 7.- Continued. (b) Mach number, 0.60.

Figure 7.- Continued. (c) Mach number, 0.80.

Figure 7.- Continued. (d) Mach number, 0.90.

Figure 7.- Concluded. (e) Mach number, 0.925.

Figure 8.- The pressure distribution over the fuselage of the MX-656 model. ψ_u , 0° ; δ_{lf} , 0°.

(a) Mach number, 0.40.

Figure 8.- Continued. (b) Mach number, 0.60.

Figure 8.- Continued. (c) Mach number 0.80.

Figure 8.- Continued. (d) Mach number, 0.90.

Figure 8.- Concluded. (e) Mach number, 0.925.

Figure 9.- The critical Mach number characteristics of the wing of the MX-656 model. ψ , 0°.

Figure 10.- The critical Mach number characteristics of the fuselage of the MX-656 model. ψ , 0°.

Figure 11.- The section normal-force characteristics of the wing of the MX-656 model. ψ , 0°.

(a) Wing station 9.02 inches.

Figure 11.- Continued. (b) Wing station 12.06 inches.

Figure 11.- Concluded. (c) Wing station 16.56 inches.

Figure 12.- The spanwise distribution of load on the wing of the MX-656 model. ψ , 0° ; δ_{lf} , 0°.

(a) Mach number, 0.40.

Figure 12.- Continued. (b) Mach number, 0.60.

Figure 12.- Continued. (c) Mach number, 0.80.

Figure 12.- Continued. (d) Mach number, 0.90.

Figure 12.-Concluded. (e) Mach number, 0.925.

Figure 13.- The spanwise distribution of load on the wing of the MX-656 model. ψ, 0° ; δ_{lf} , 30°.

(a) Mach number, 0.40.

Figure 13.- Continued. (b) Mach number, 0.60.

Figure 13.- Continued. (c) Mach number, 0.80.

Figure 13.- Continued. (d) Mach number, 0.90.

Figure 13.- Concluded. (e) Mach number, 0.925.

Figure 14.- The velocity ratio in the fuselage boundary layer of the MX-656 model at station 43.2 inches. ψ_u , 0° .

Figure 15.- The pressure distribution over the wing of the MX-656 model. α_u , 6.2° ; δ_{lf} , 0° .

(a) Mach number, 0.40.

Figure 15.- Continued. (b) Mach number, 0.60.

Figure 15.- Continued. (c) Mach number, 0.80.

Figure 15.- Concluded. (d) Mach number, 0.90.

Figure 16.- The pressure distribution over the fuselage of the MX-656 model. α_u , 6.2° ; δ_{lf} , 0°.

(a) Mach number, 0.40.

Figure 16.- Continued. (b) Mach number, 0.60.

Figure 16.- Continued. (c) Mach number, 0.80.

Figure 16.- Concluded. (d) Mach number, 0.90.

Figure 17.- The velocity ratio in the fuselage boundary layer of the MX-656 model at station 43.2 inches. α_u , 6.2°.

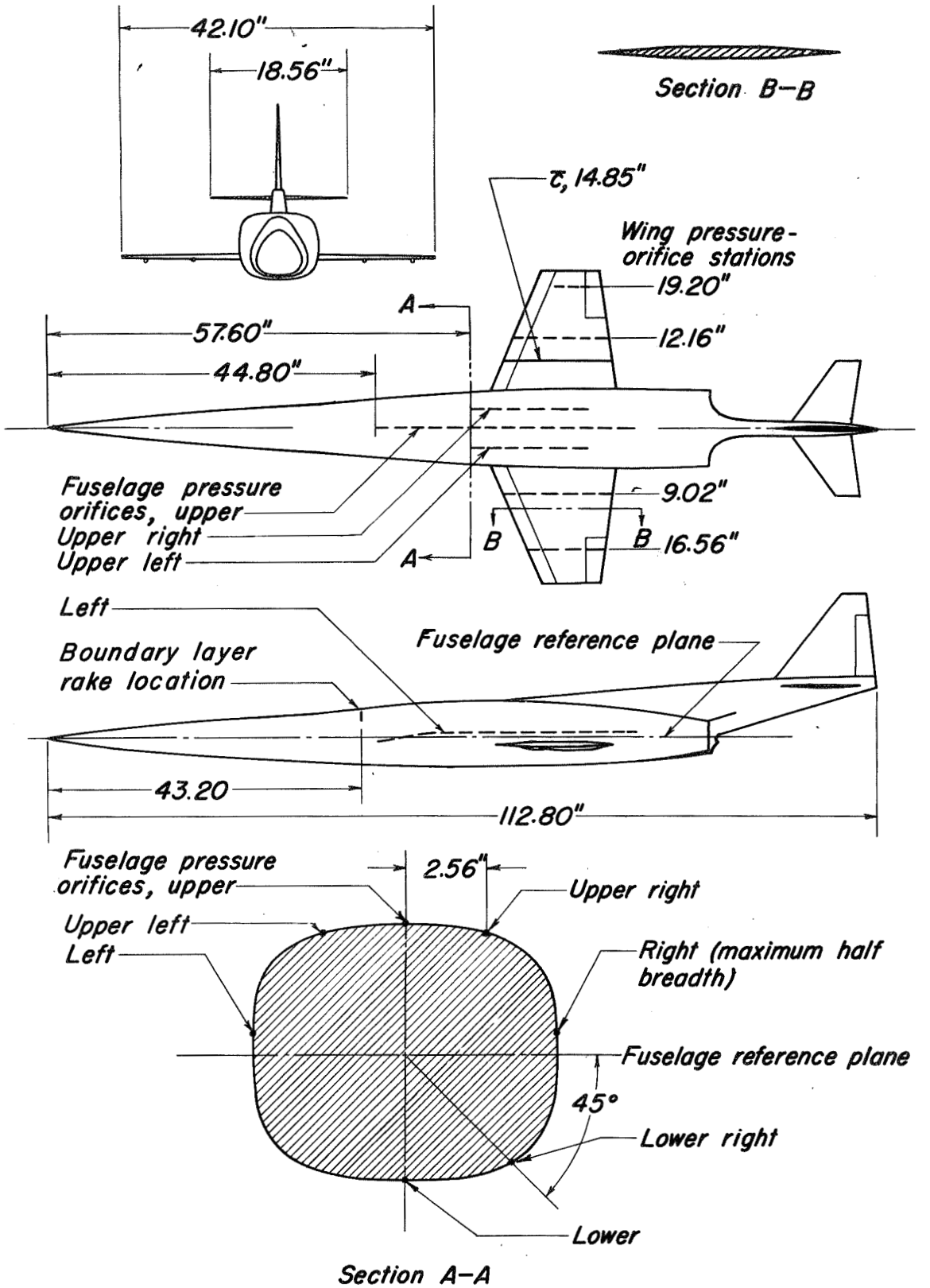

Figure 1.–The location of the pressure-orifice stations on the wing and fuselage of the MX-656 model.

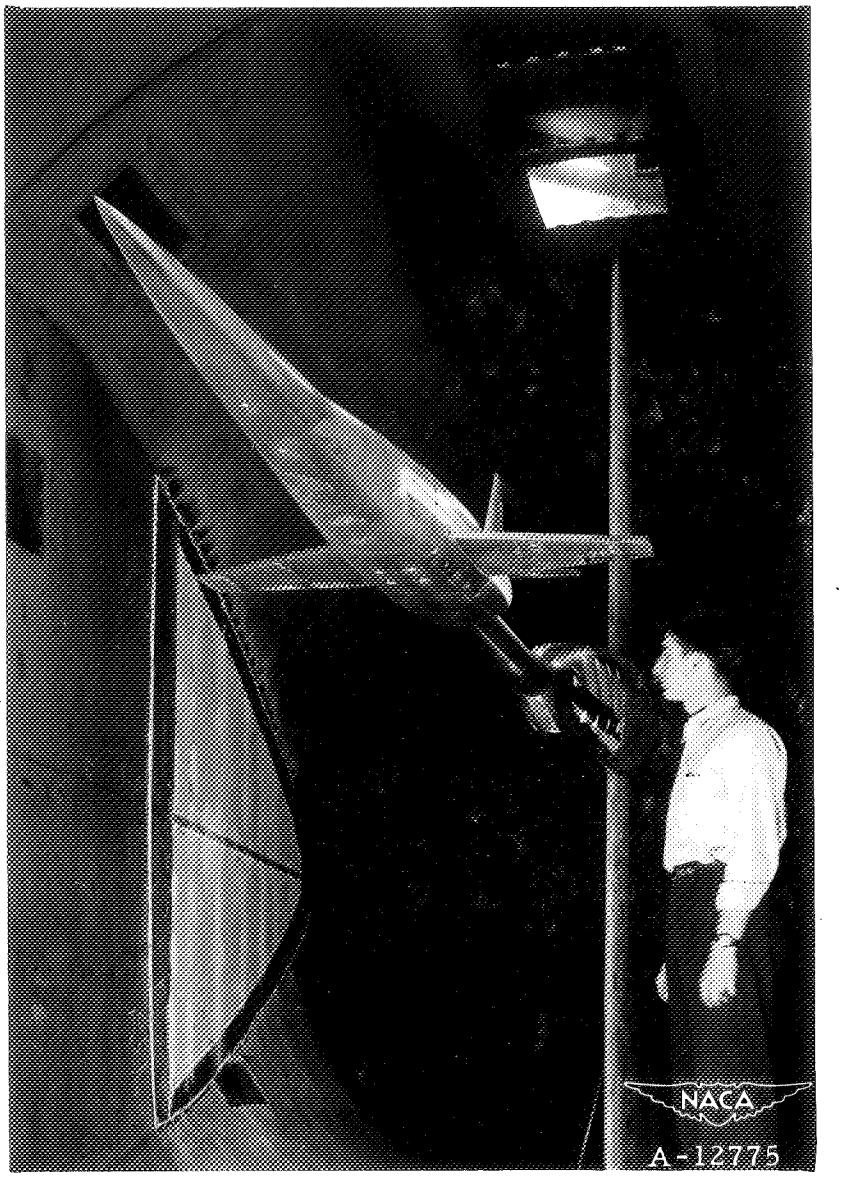

Figure 2. – The MX–656 model mounted in the Ames 16–foot high–speed wind tunnel for pressure–distribution tests in pitch.

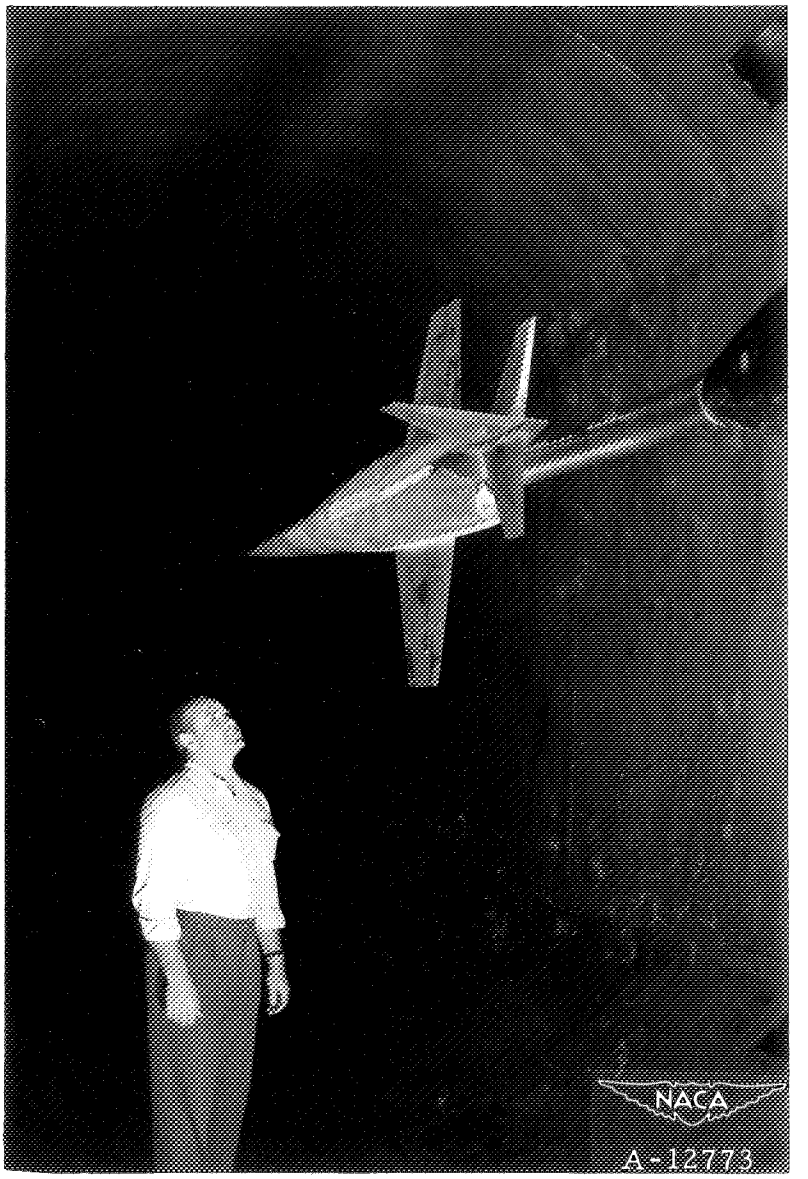

Figure 3. – The MX–656 Model mounted in the Ames 16–foot high–speed wind tunnel for pressure–distribution tests in yaw.

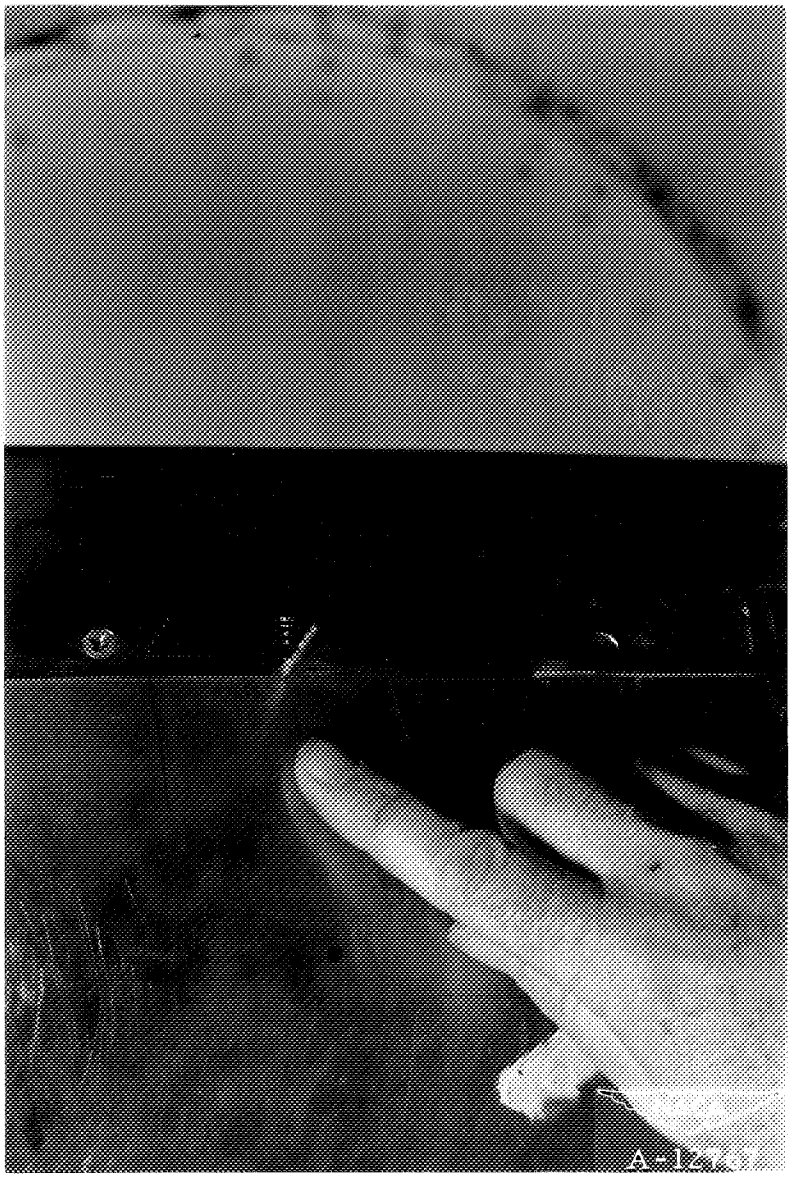

Figure 4.- The fuselage boundary-layer rake mounted on the MX-656 model.

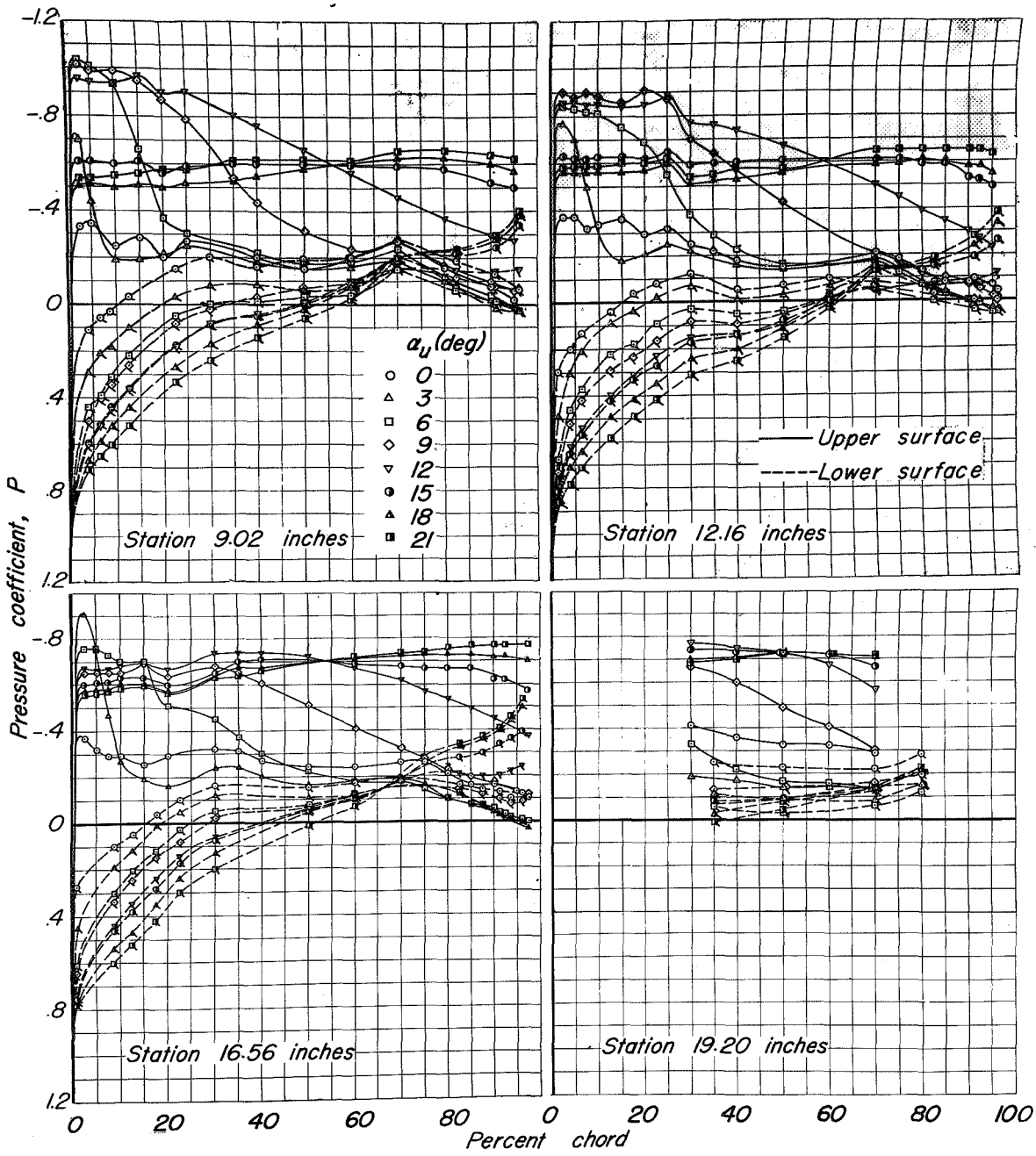

(a) Mach number, 0.40.

Figure 5.-The pressure distribution over the wing of the MX-656 model. ψ, 0°; δ_{lf}, 0°.

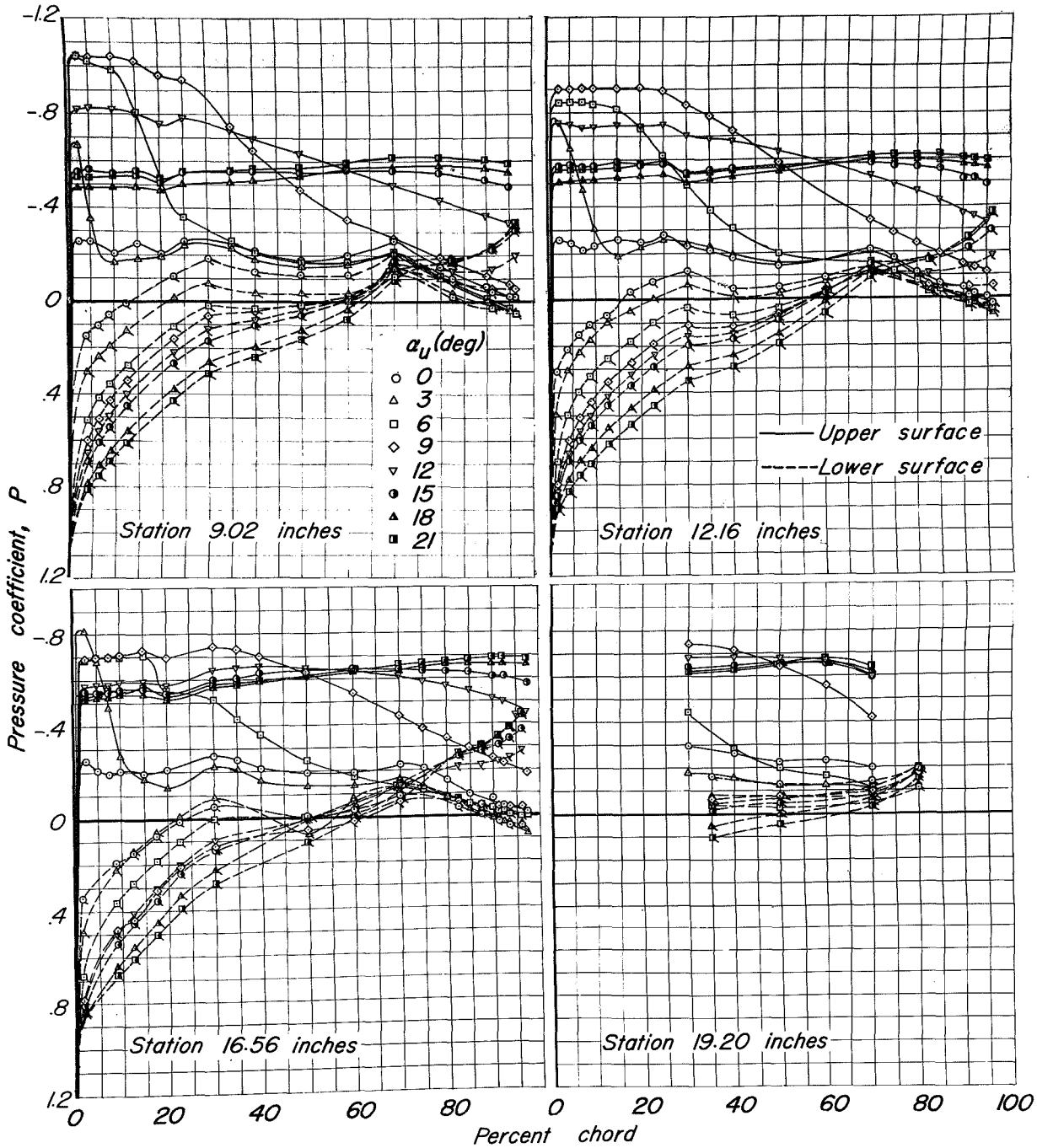

(b) Mach number, 0.60.

Figure 5.- Continued.

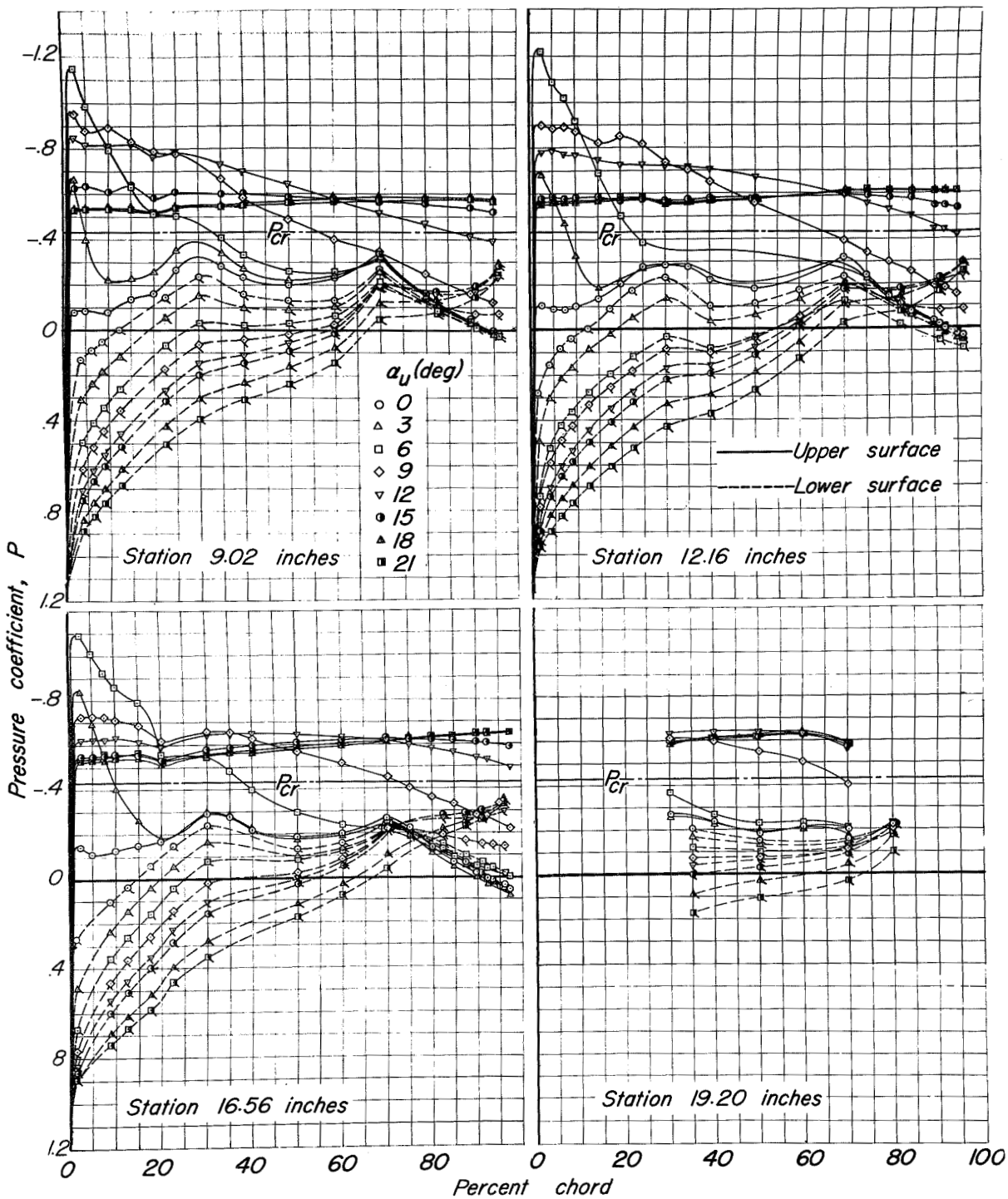

(c) Mach number 0.80.

Figure 5.-Continued.

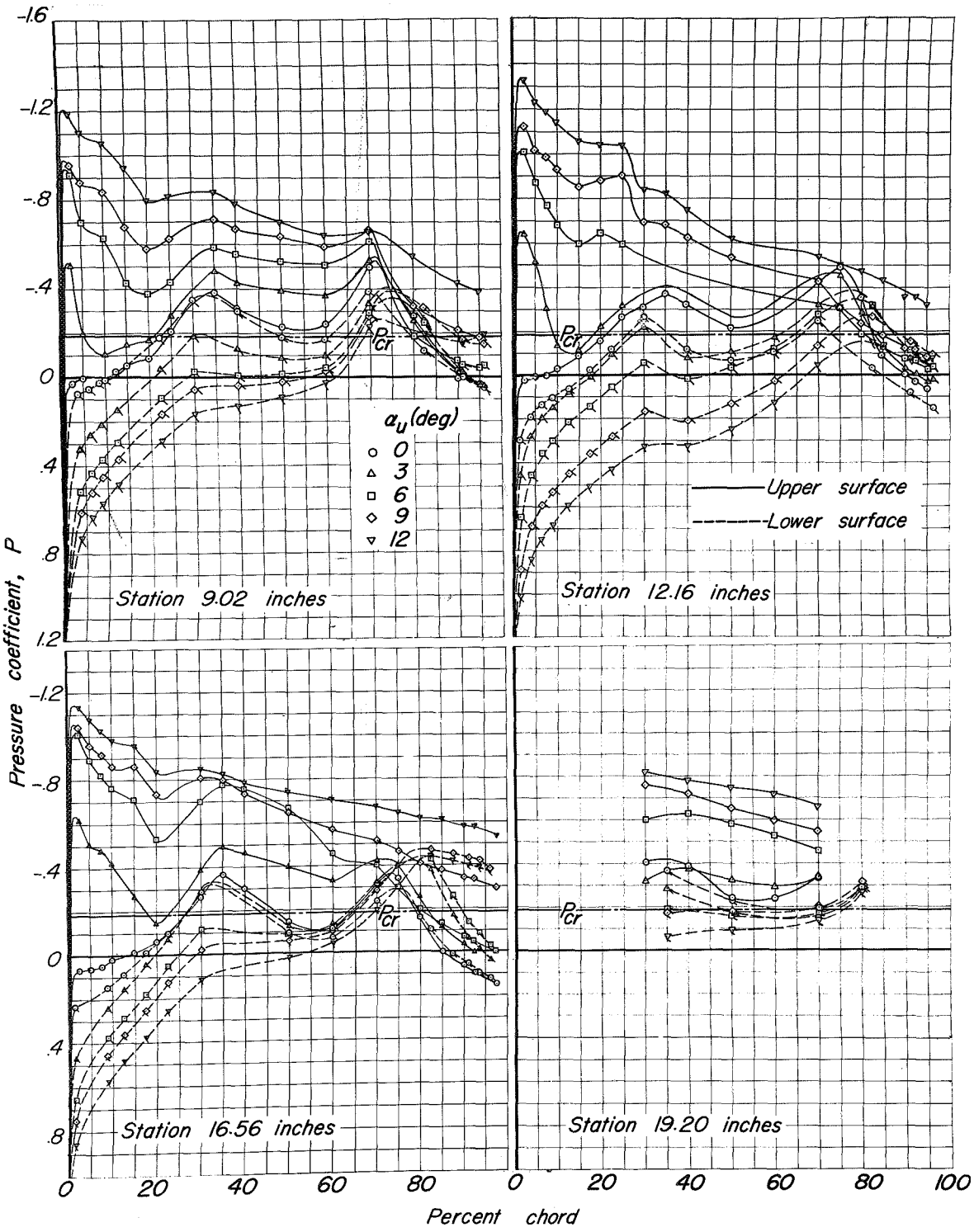

(d) Mach number, 0.90.

Figure 5.-Continued.

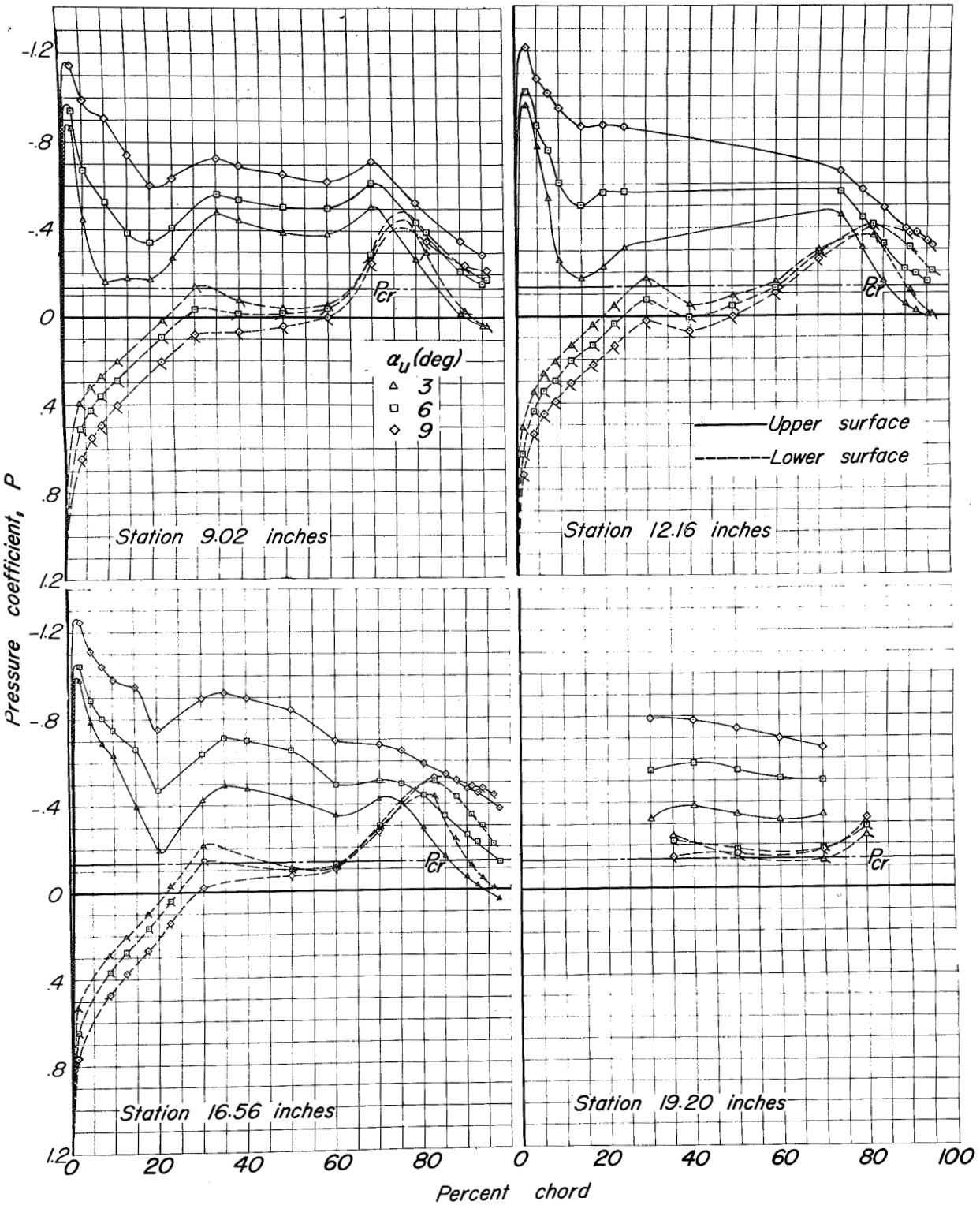

(e) Mach number, 0.925.

Figure 5.-Concluded.

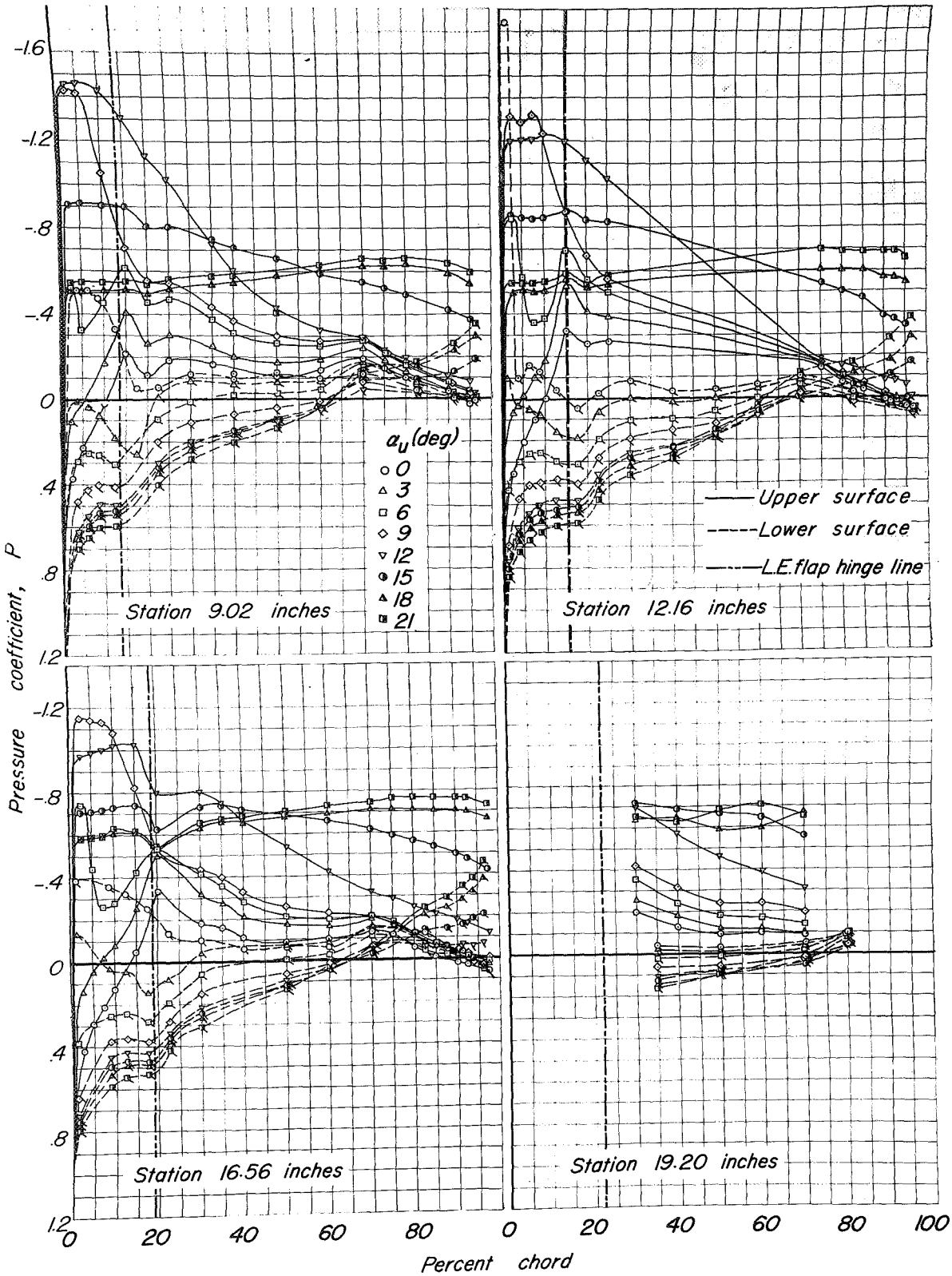

(a) Mach number, 0.40.

Figure 6.- The pressure distribution over the wing of the MX-656 model. ψ, 0°; δ_{lf}, 10°.

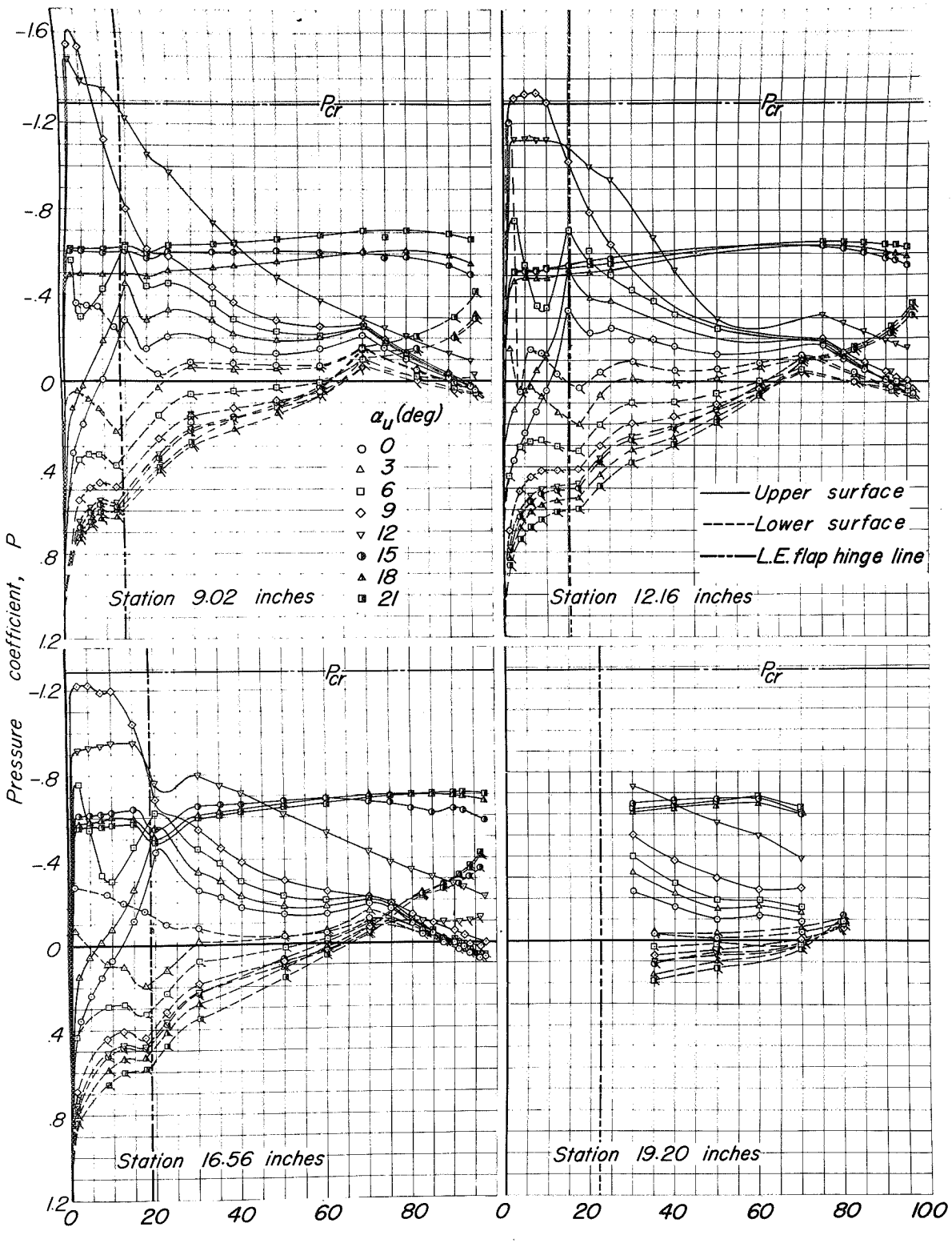

(b) Mach number, 0.60.

Figure 6.–Continued.

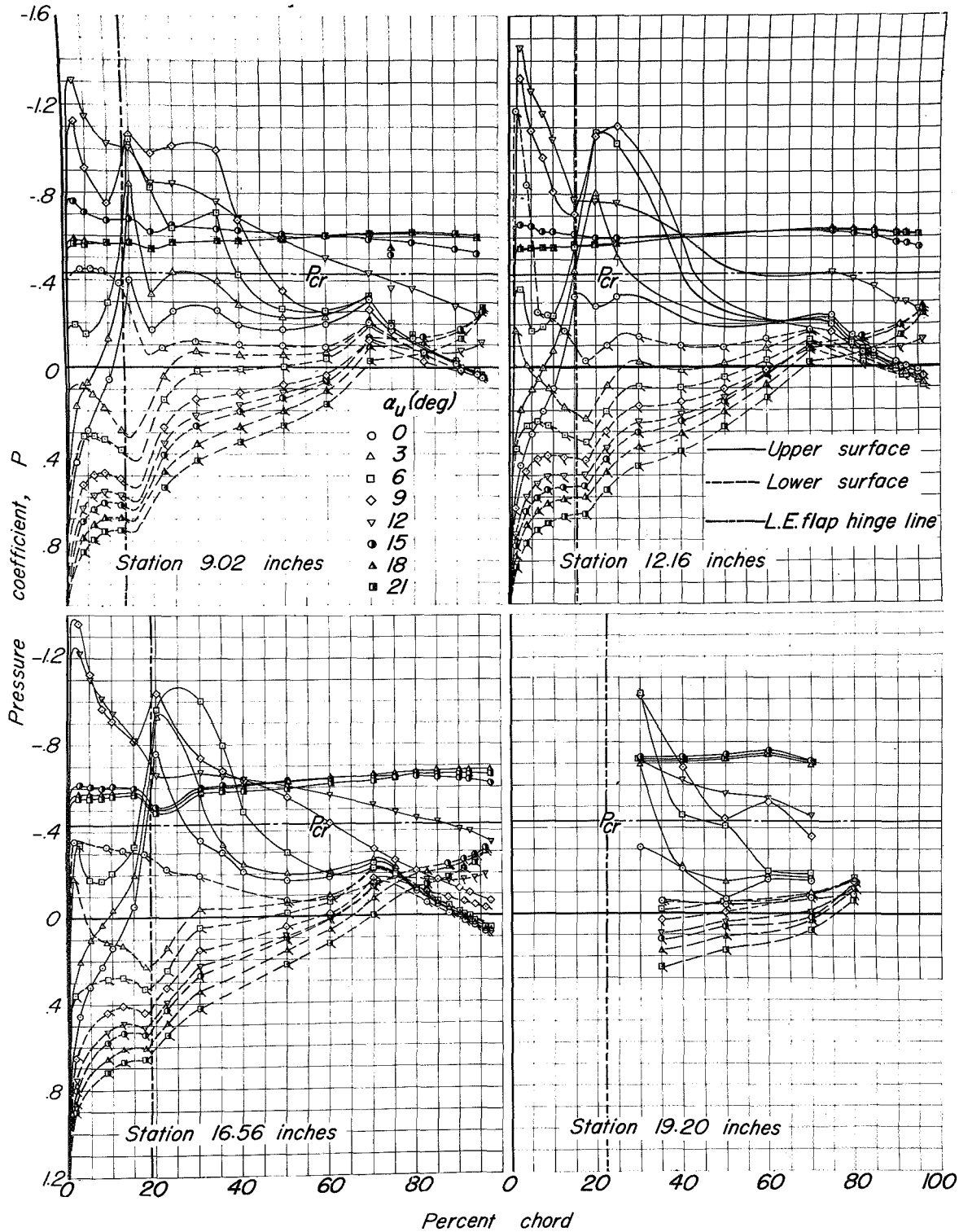

(c) Mach number 0.80.

Figure 6.–Continued.

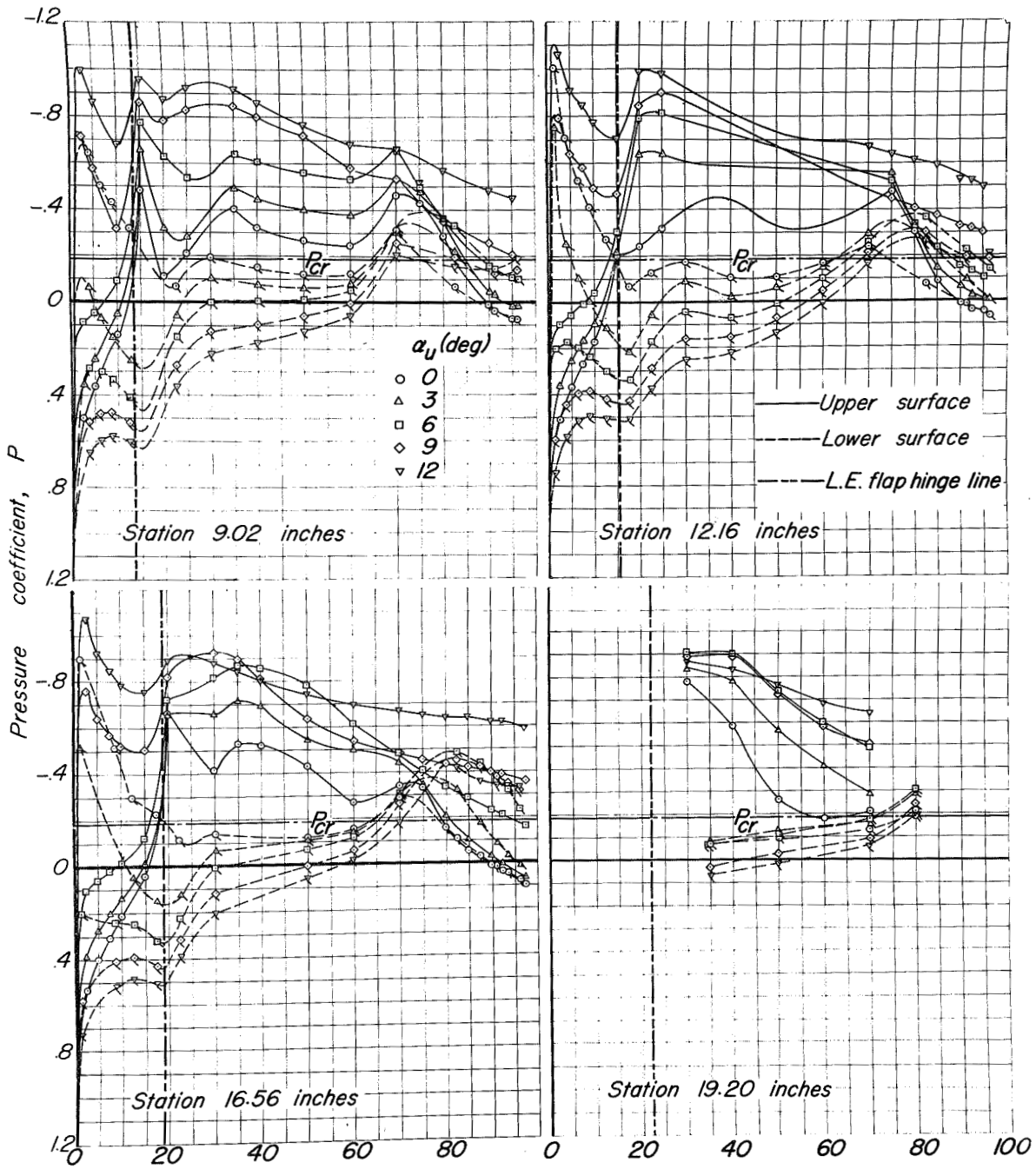

(d) Mach number, 0.90.

Figure 6.—Continued.

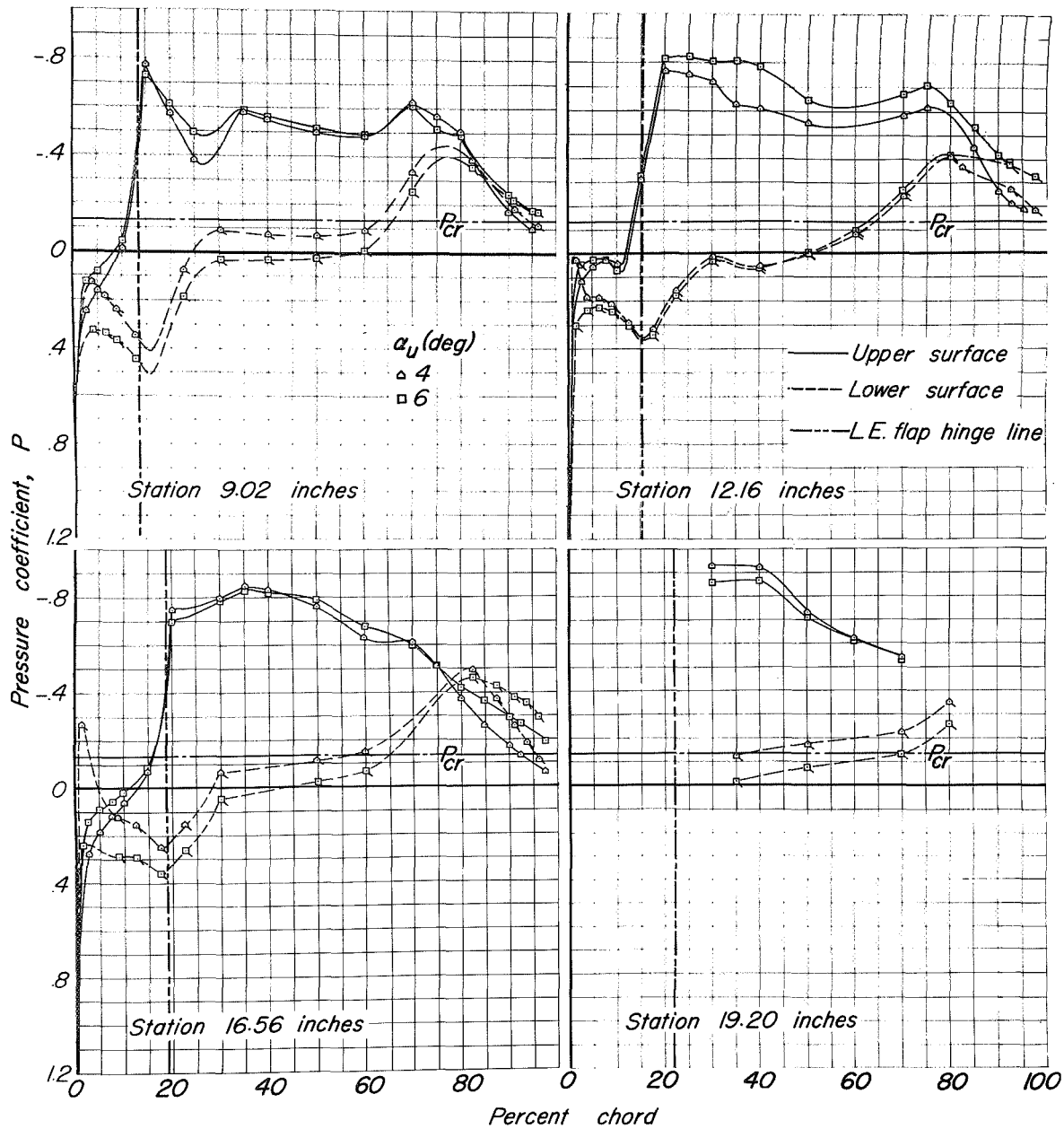

(e) Mach number, 0.925.

Figure 6.- Concluded.

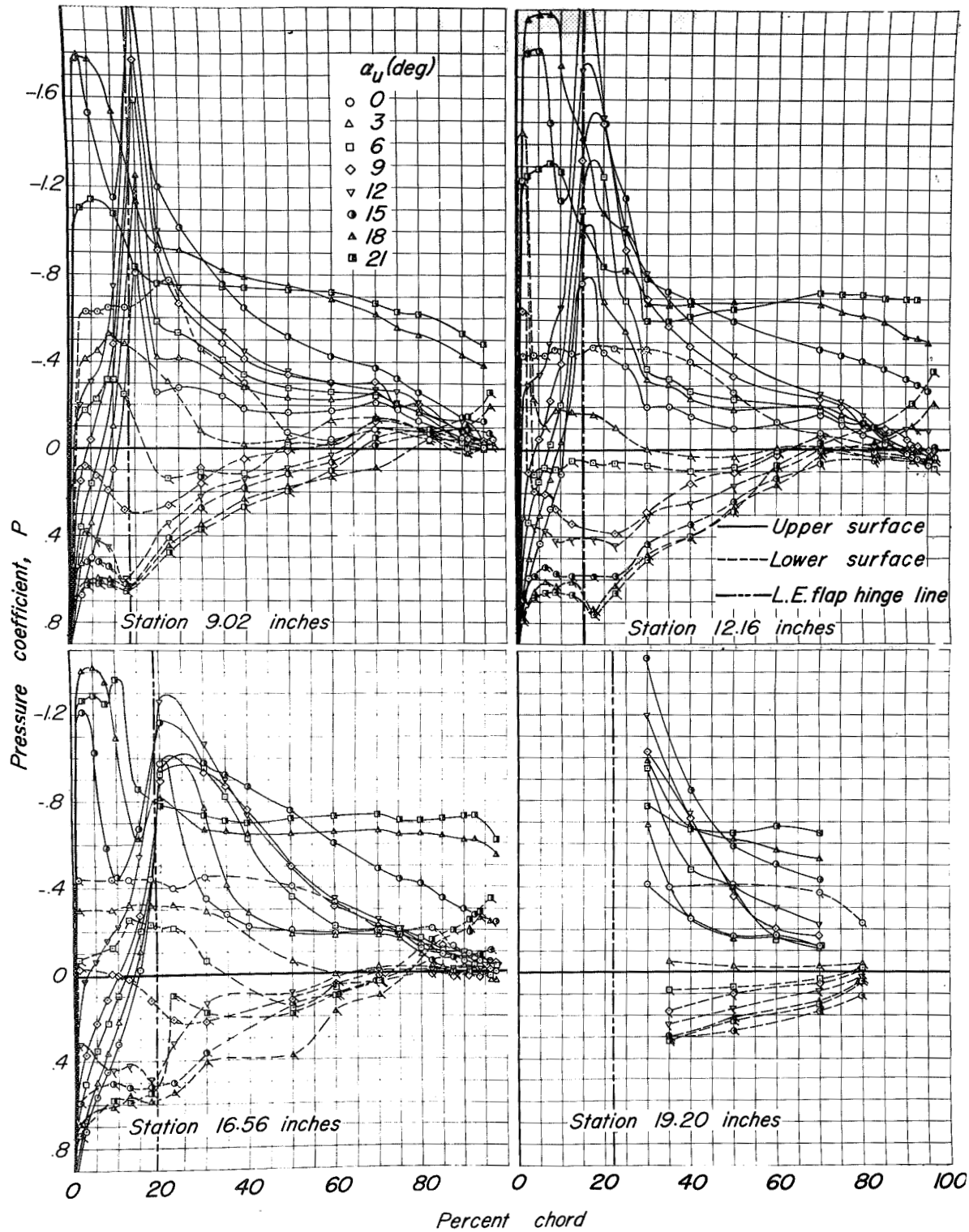

(a) Mach number, 0.40.

Figure 7.- The pressure distribution over the wing of the MX-656 model. ψ, 0°; δ_{1f}, 30°.

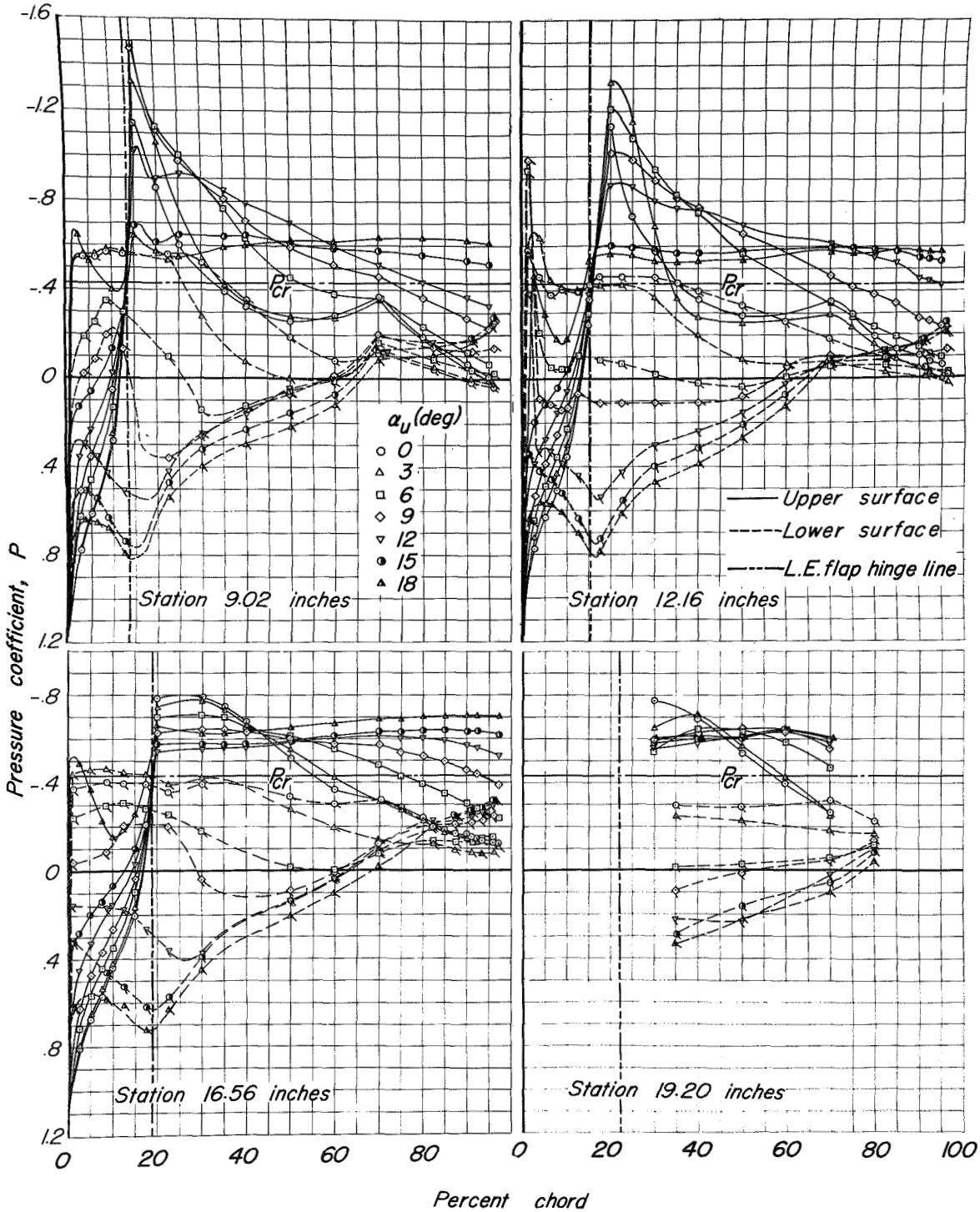

(c) Mach number 0.80.

Figure 7.—Continued.

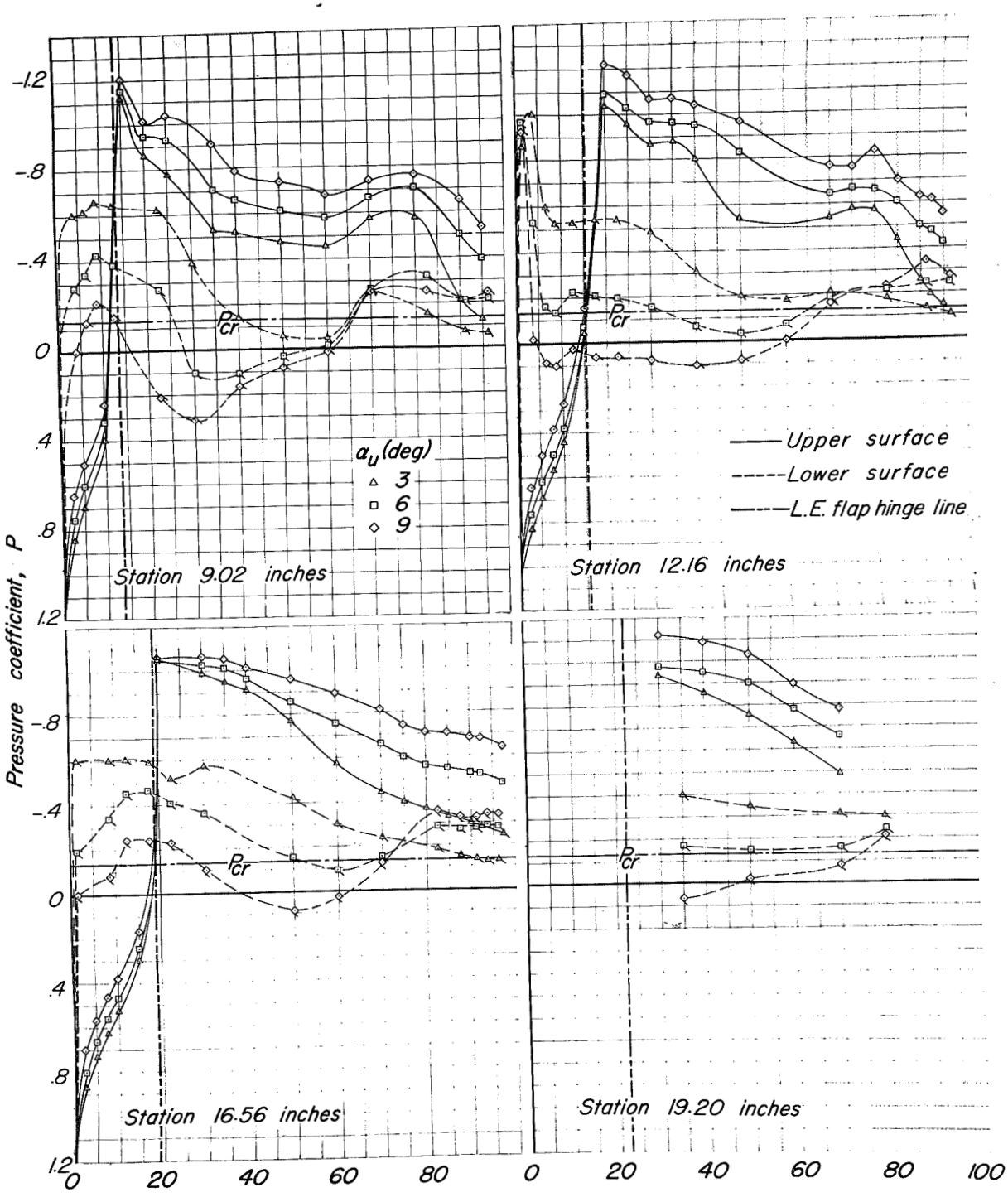

(e) Mach number, 0.925.

Figure 7.—Concluded.

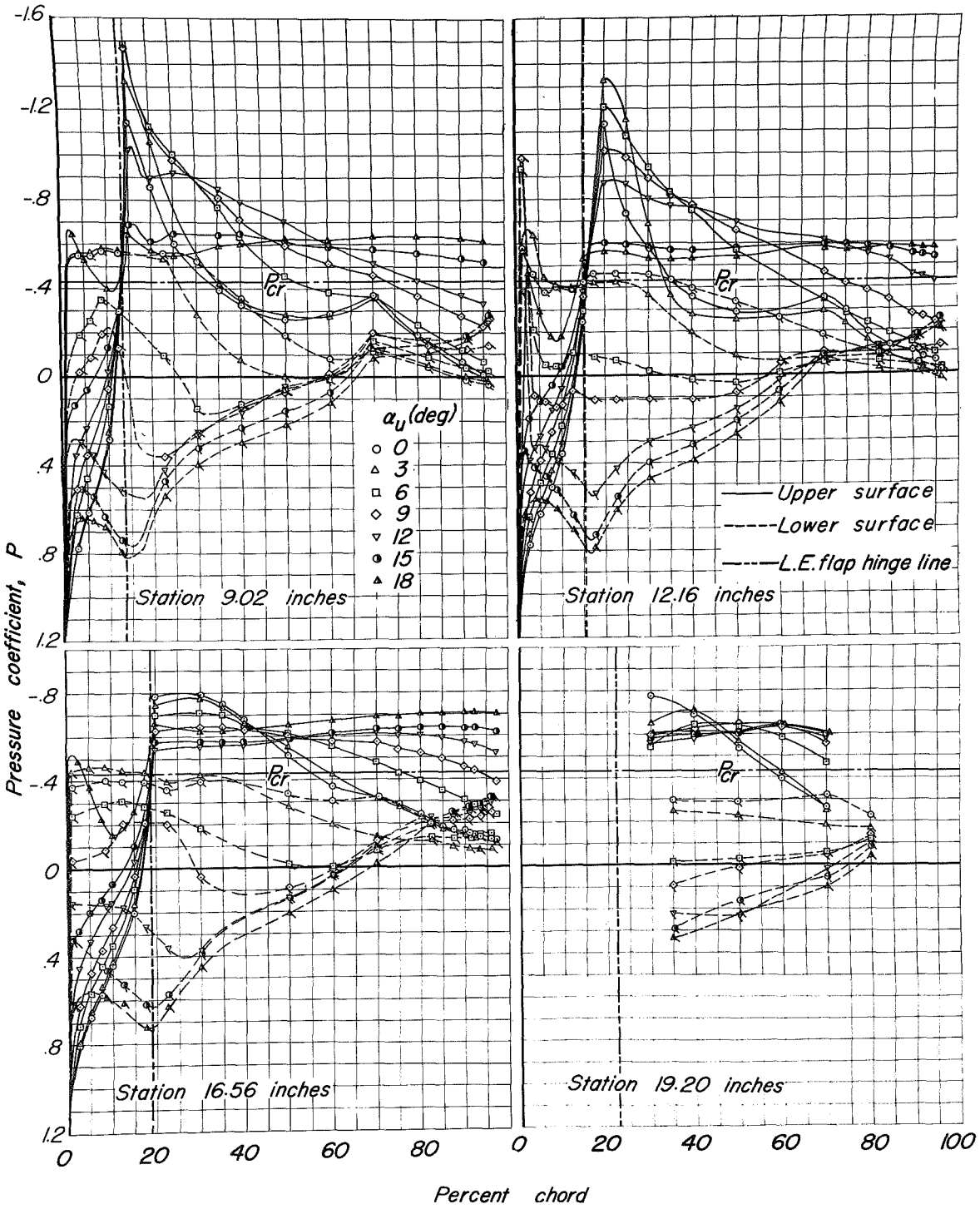

(c) Mach number 0.80.

Figure 7.—Continued.

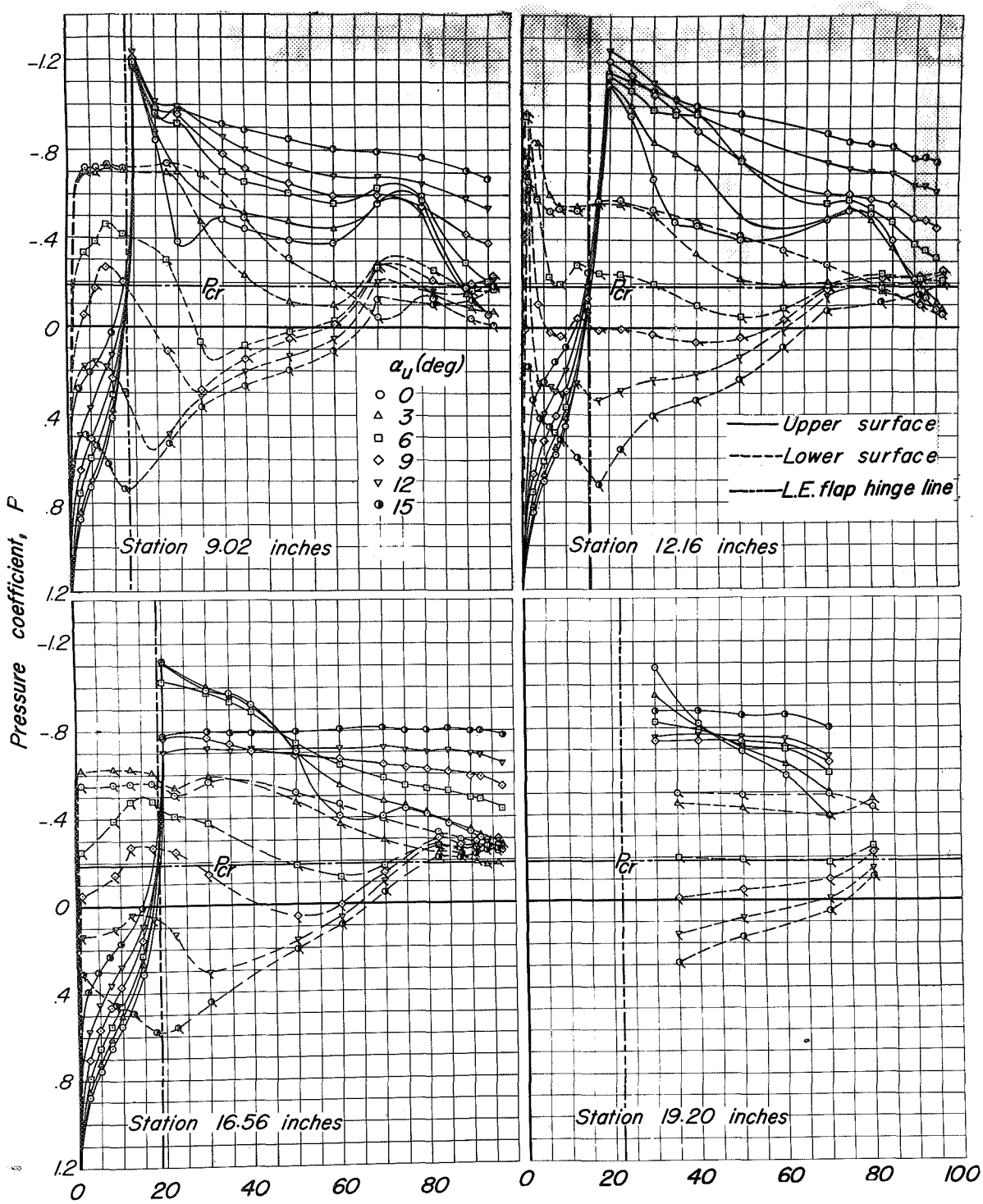

(d) Mach number, 0.90.

Figure 7.- Continued.

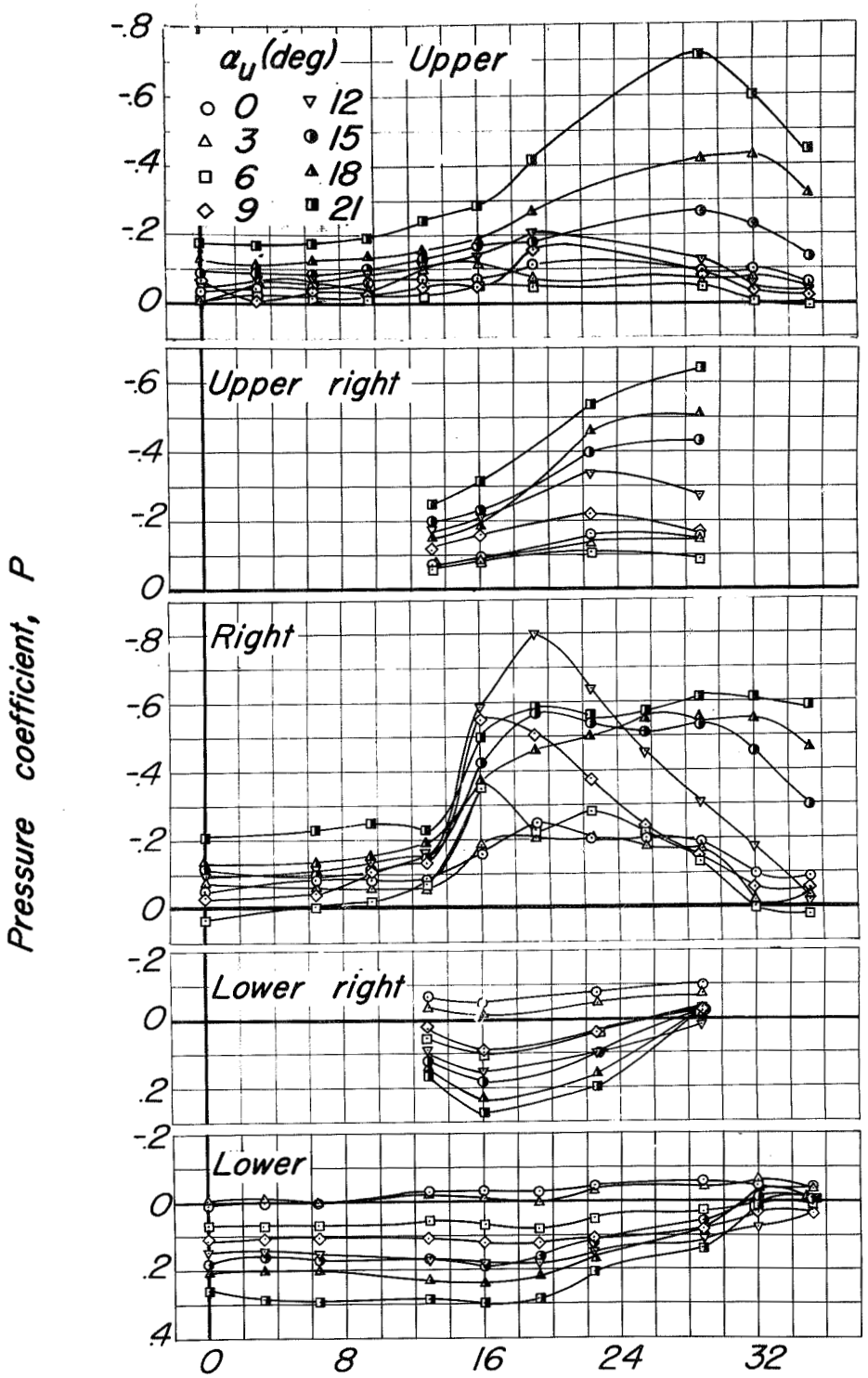

(a) Mach number, 0.40.

Figure 8.-The pressure distribution over the fuselage of the MX-656 model. ψ_u, 0°; δ_{lf}, 0°.

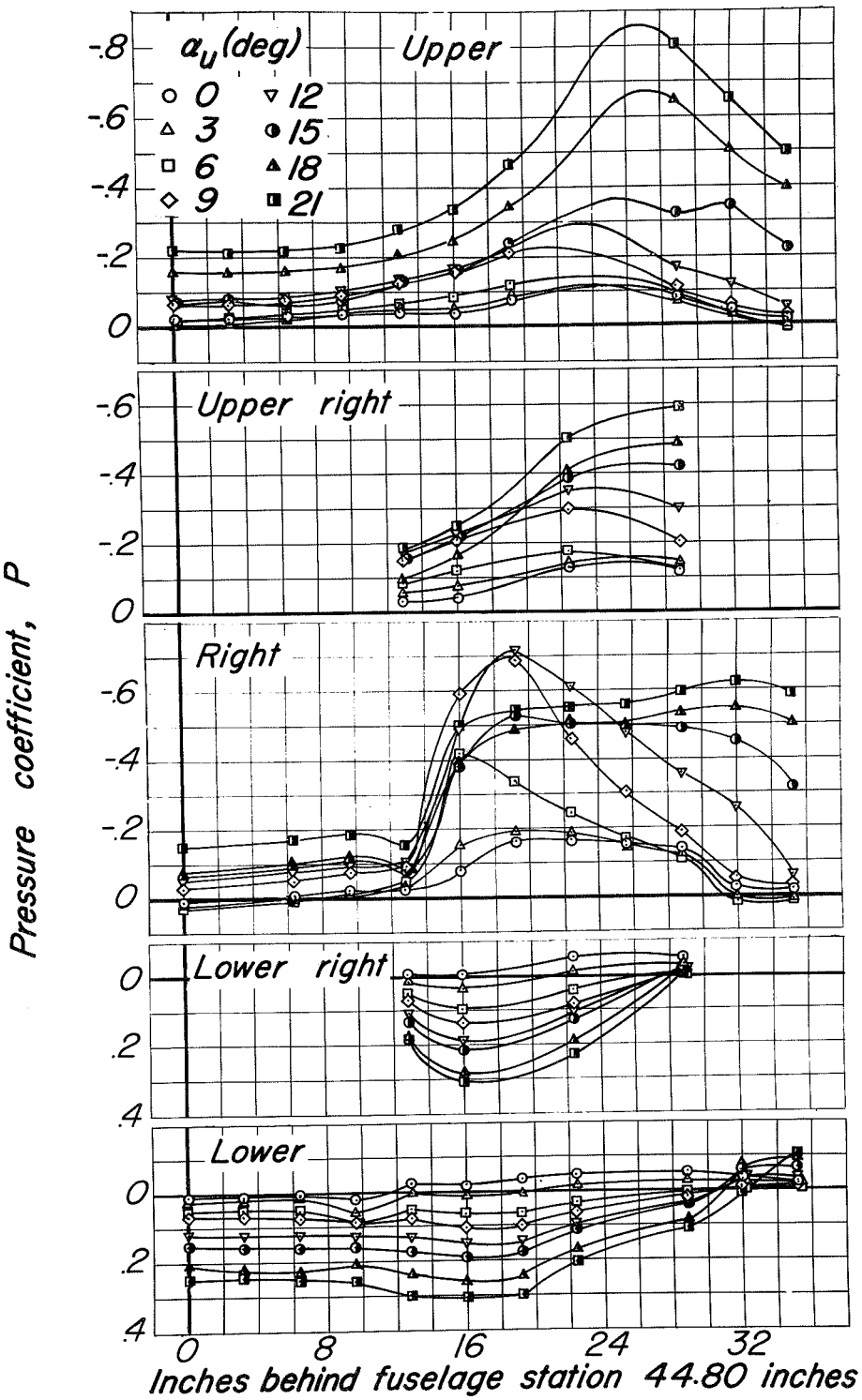

(b) Mach number, 0.60.

Figure 8.- Continued.

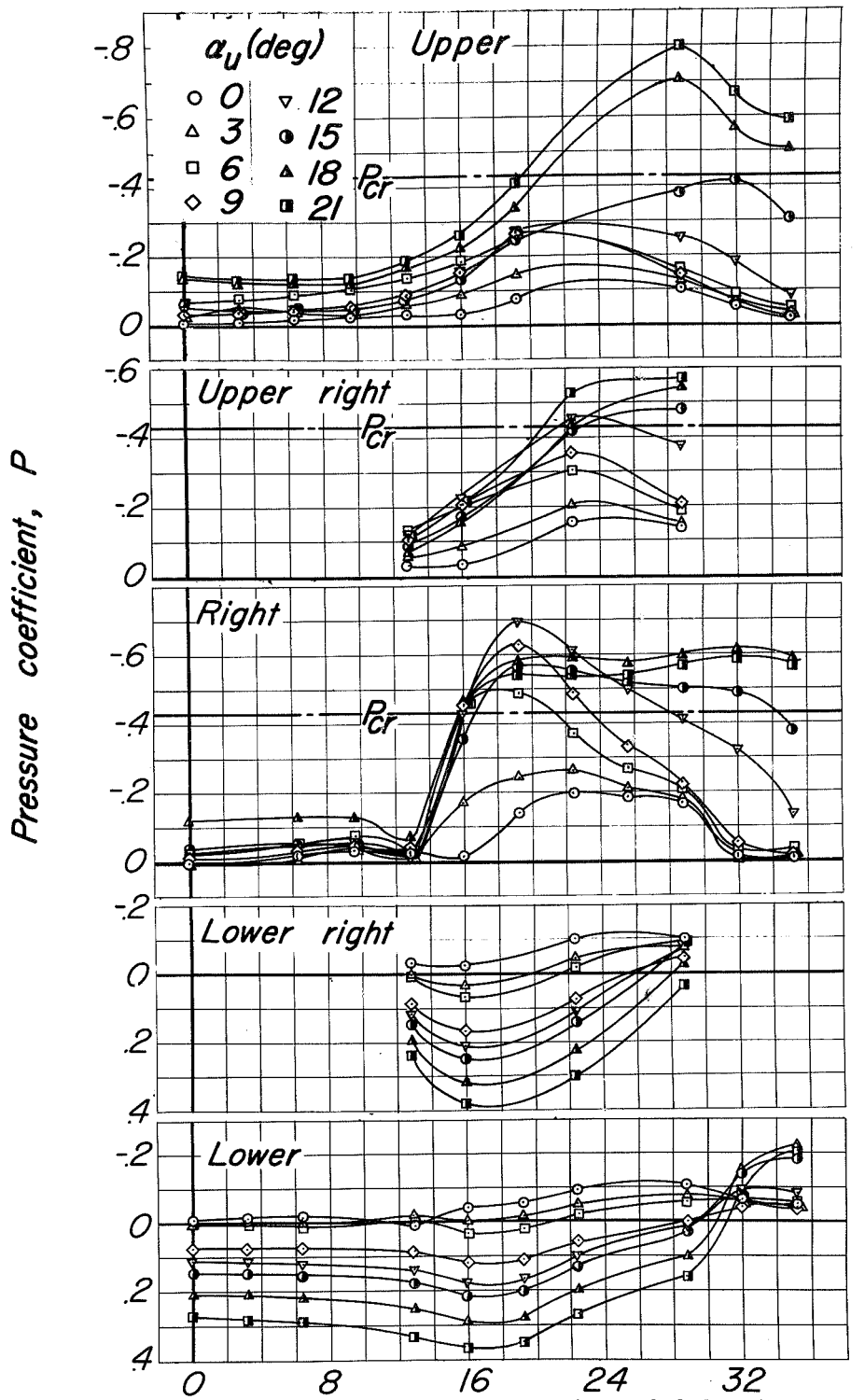

(c) Mach number 0.80.

Figure 8.- Continued.

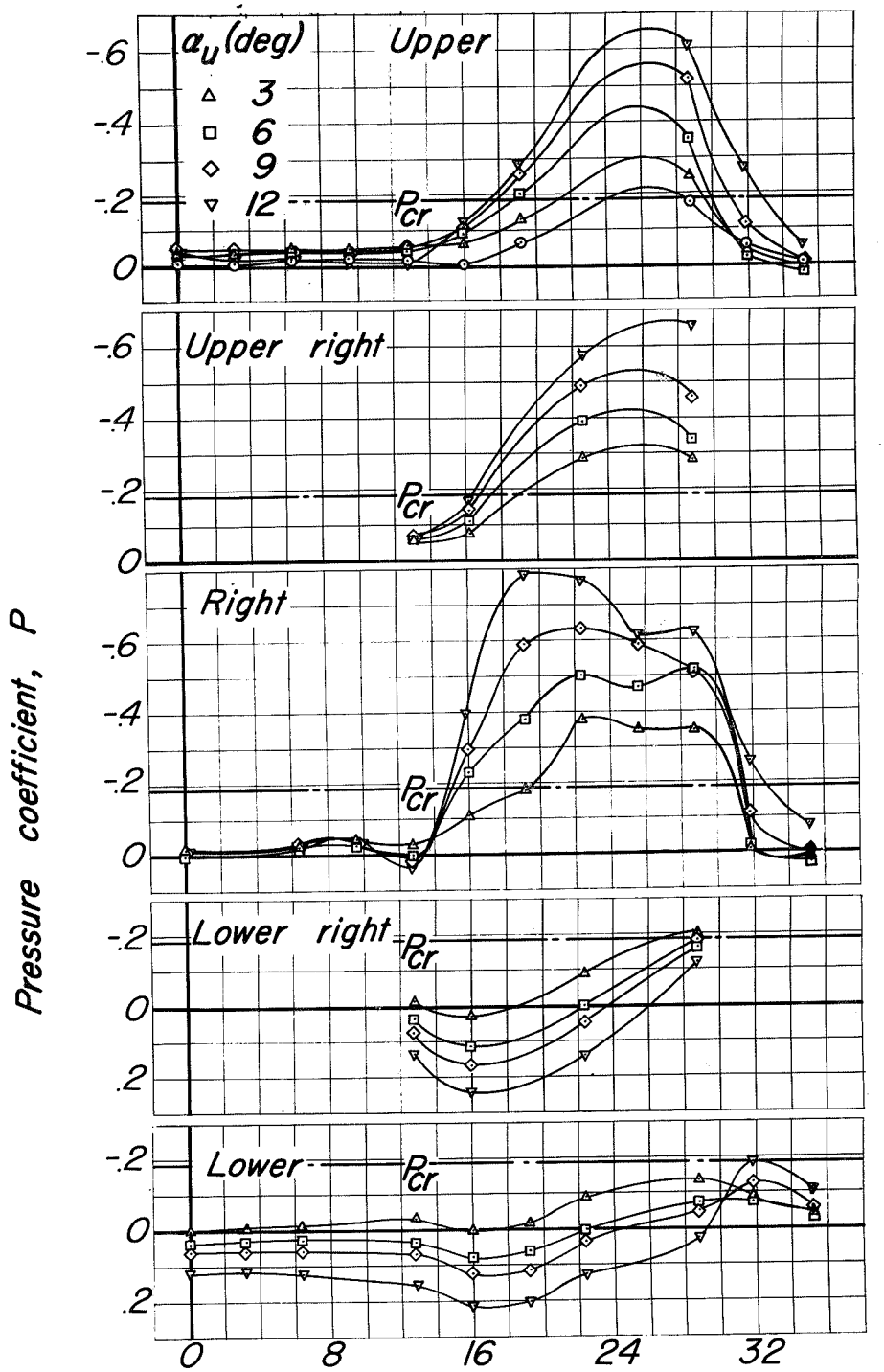

(d) Mach number, 0.90.

Figure 8.—Continued.

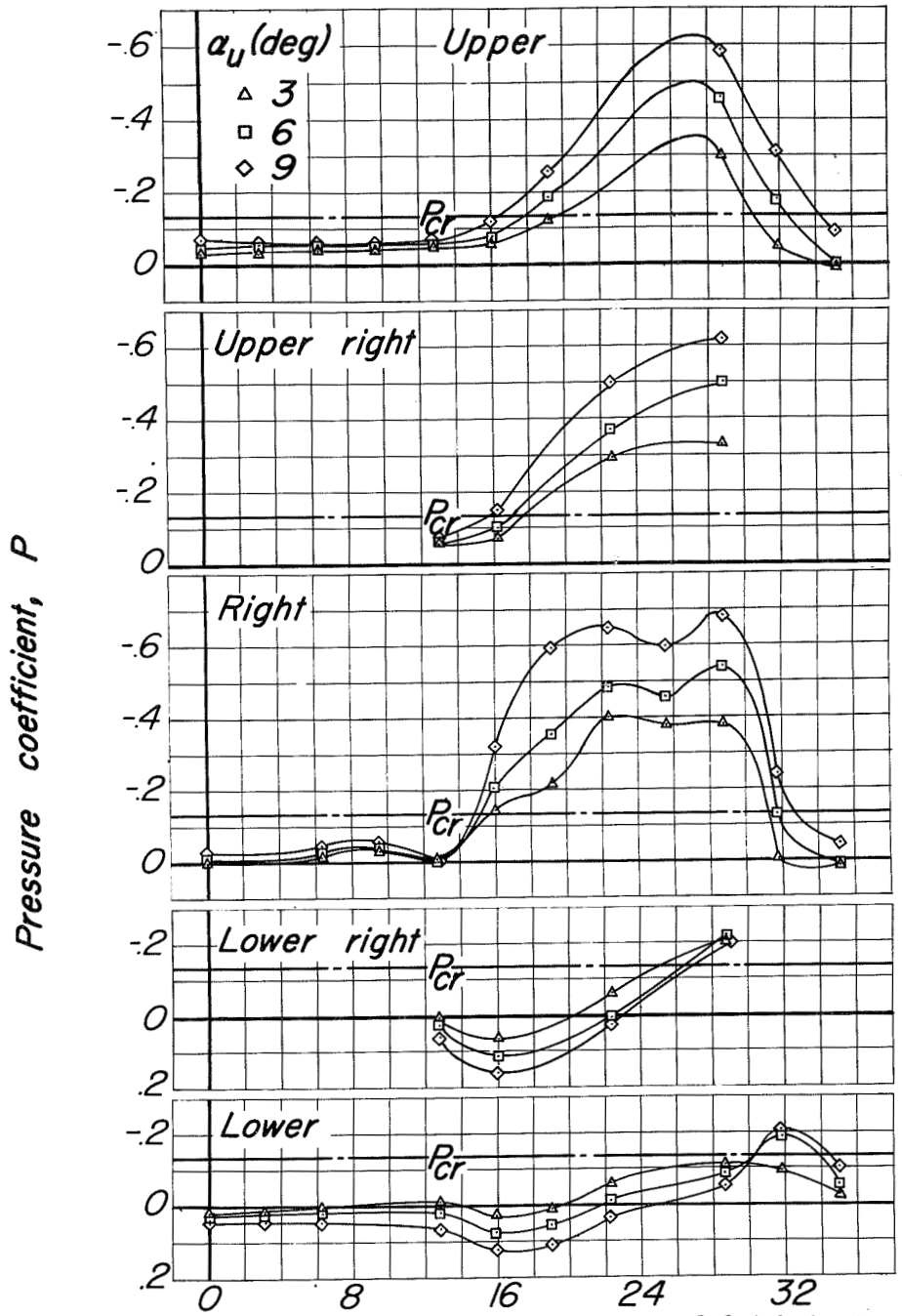

(e) Mach number, 0.925.

Figure 8.- Concluded.

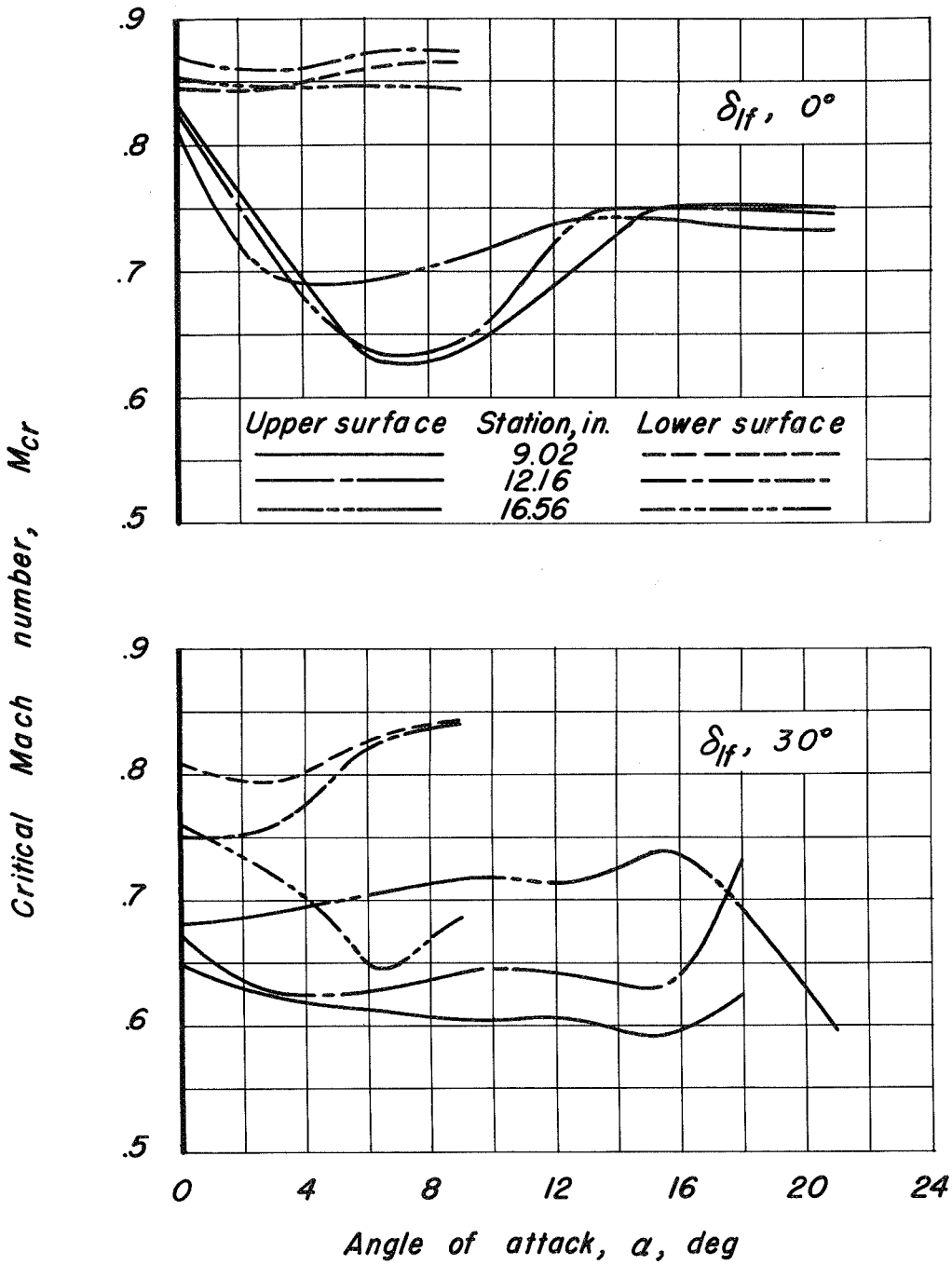

Figure 9.–The critical Mach number characteristics of the wing of the MX-656 model. ψ, 0°.

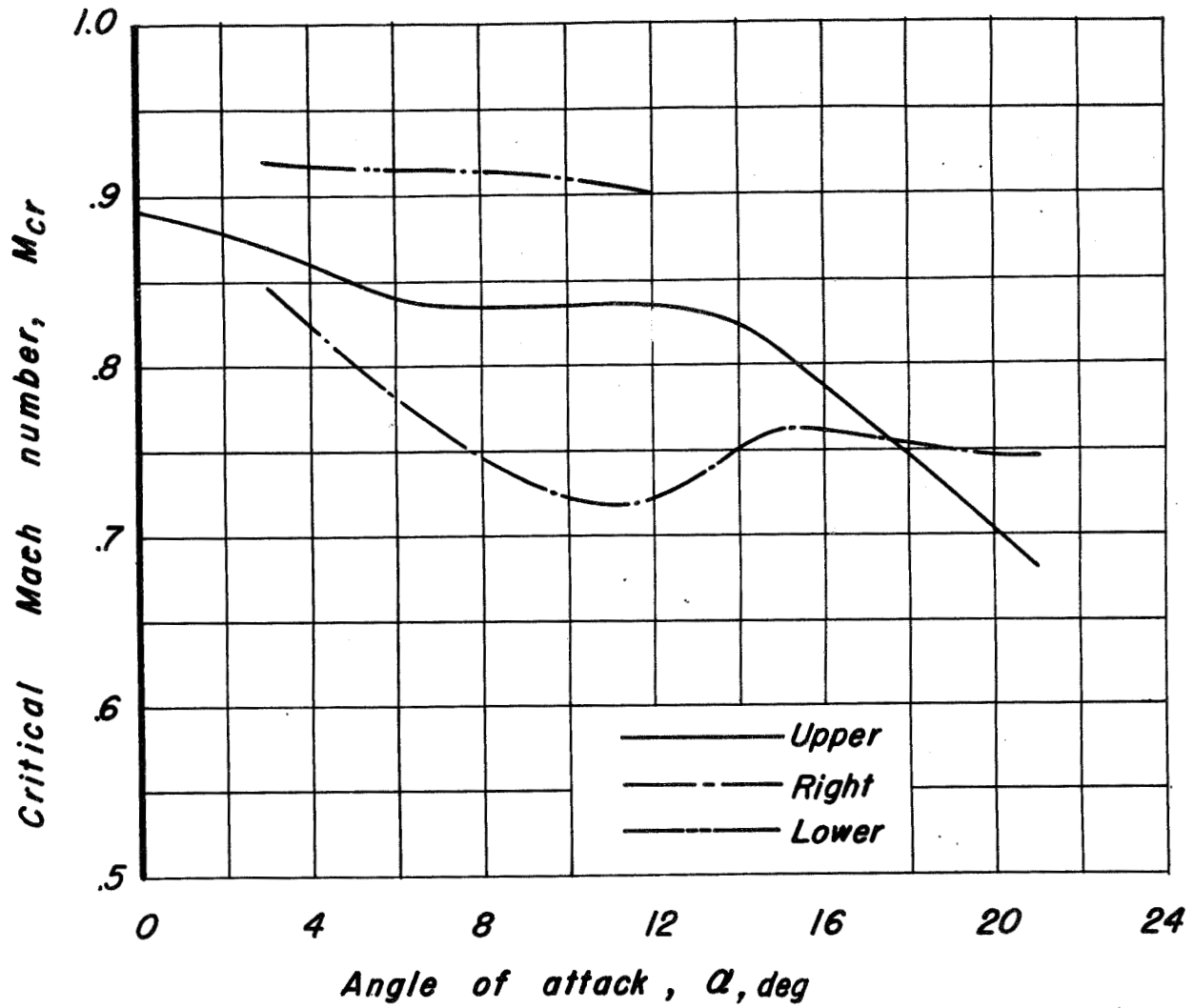

Figure 10.-The critical Mach number characteristics of the fuselage of the MX-656 model. ψ,0°

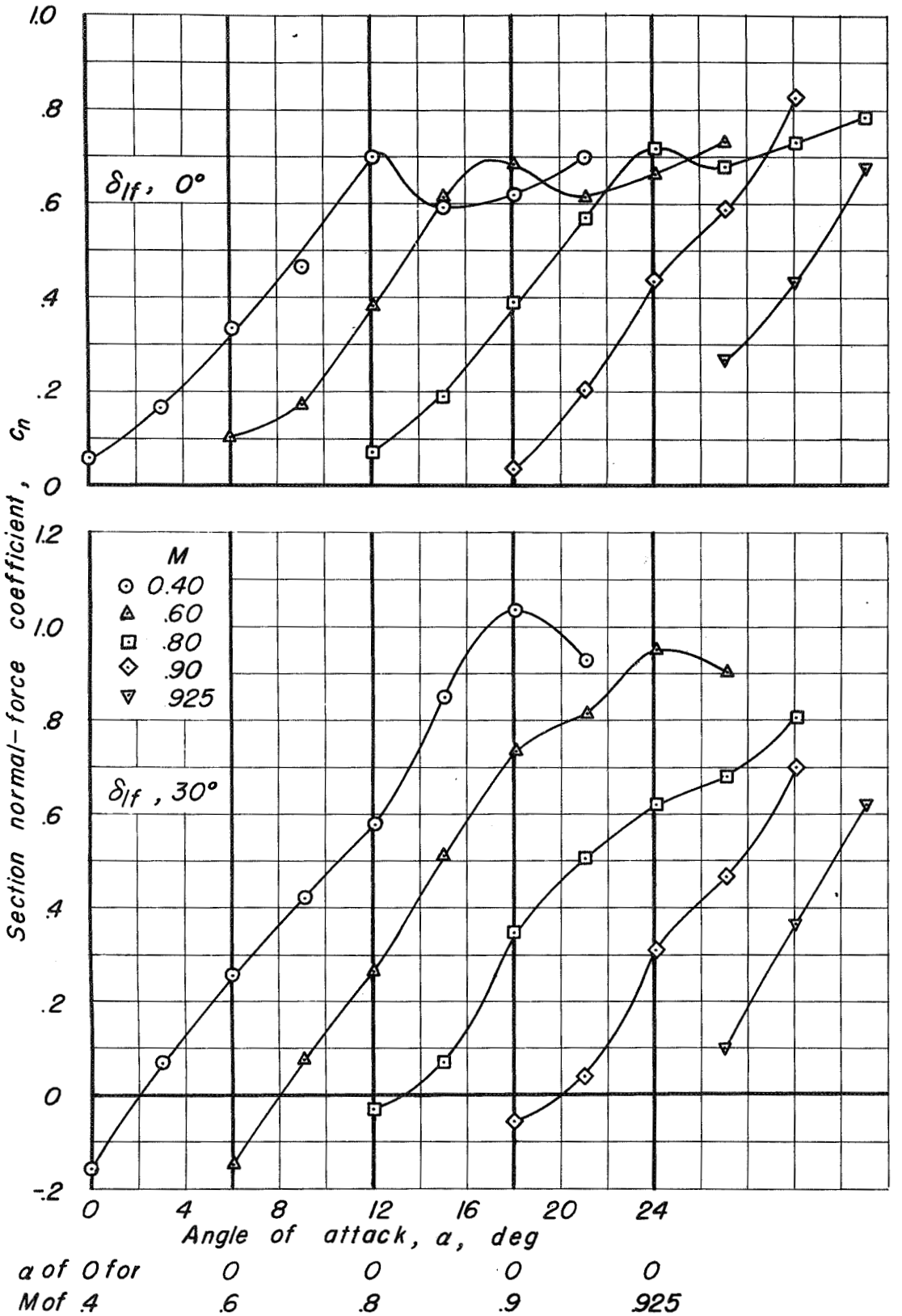

(a) Wing station 9.02 inches

Figure 11.- The section normal-force characteristics of the wing of the MX-656 model. ψ, 0°.

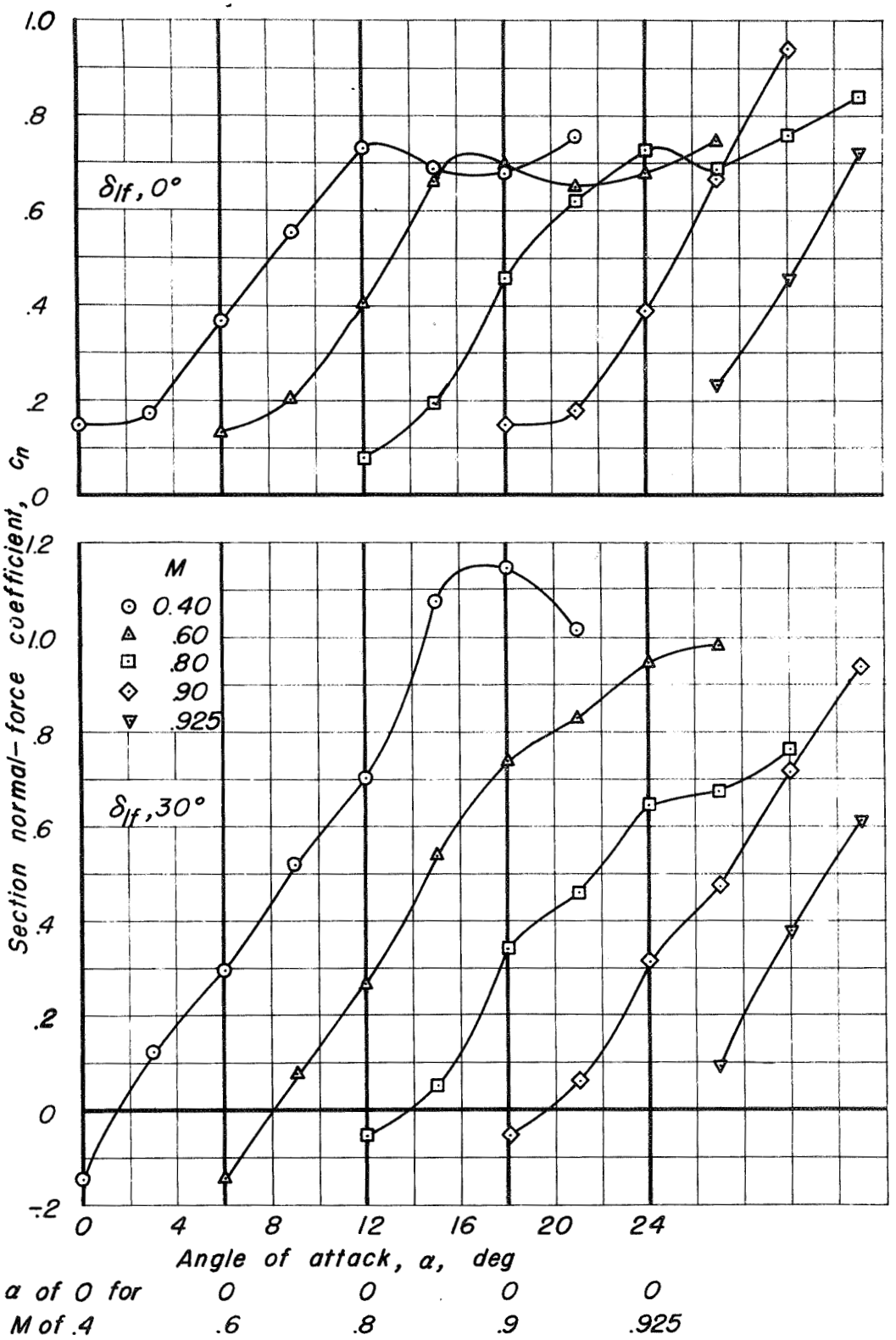

(b) Wing station 12.16 inches.
Figure 11.- Continued.

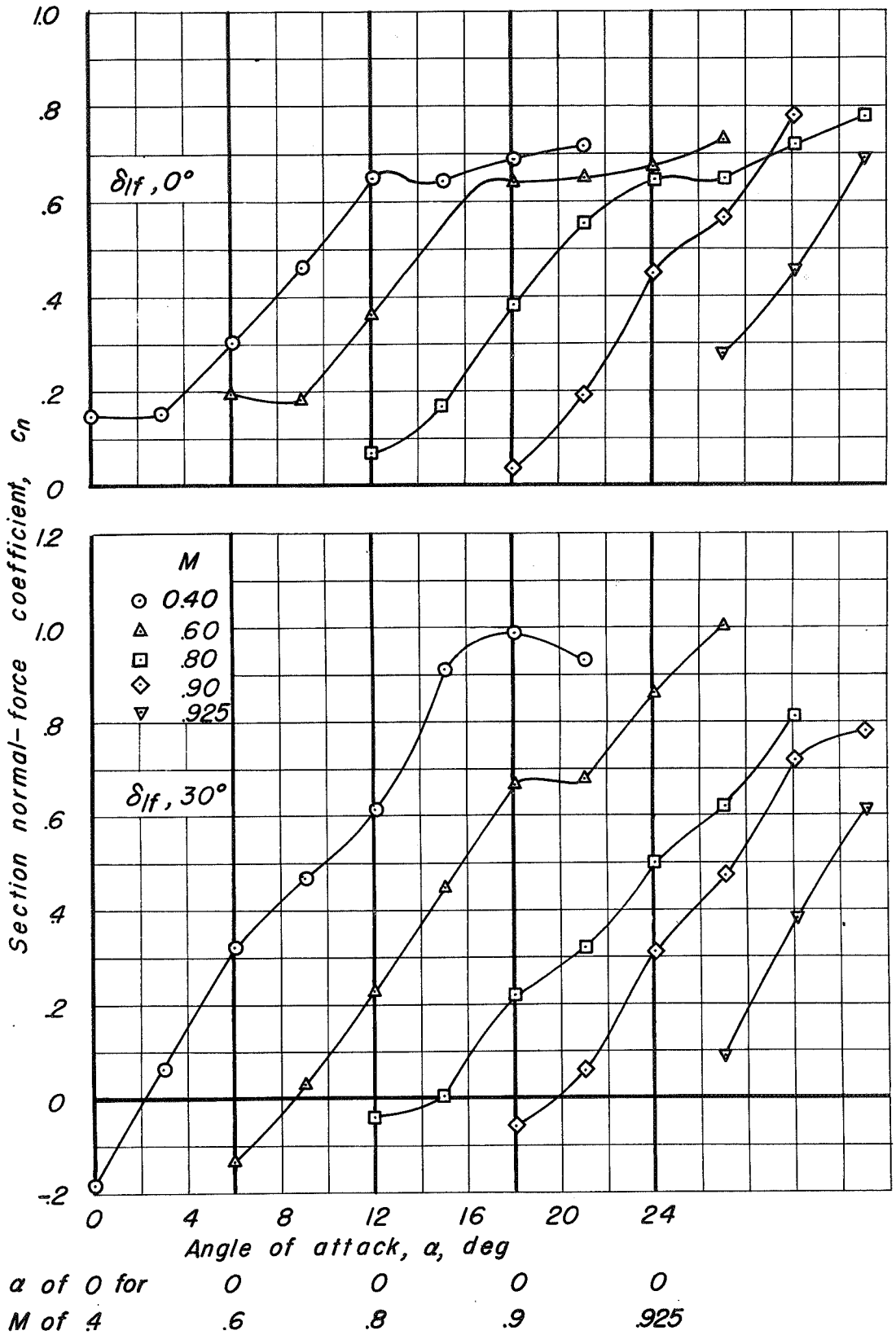

(c) Wing station 16.56 inches.

Figure 11.- Concluded.

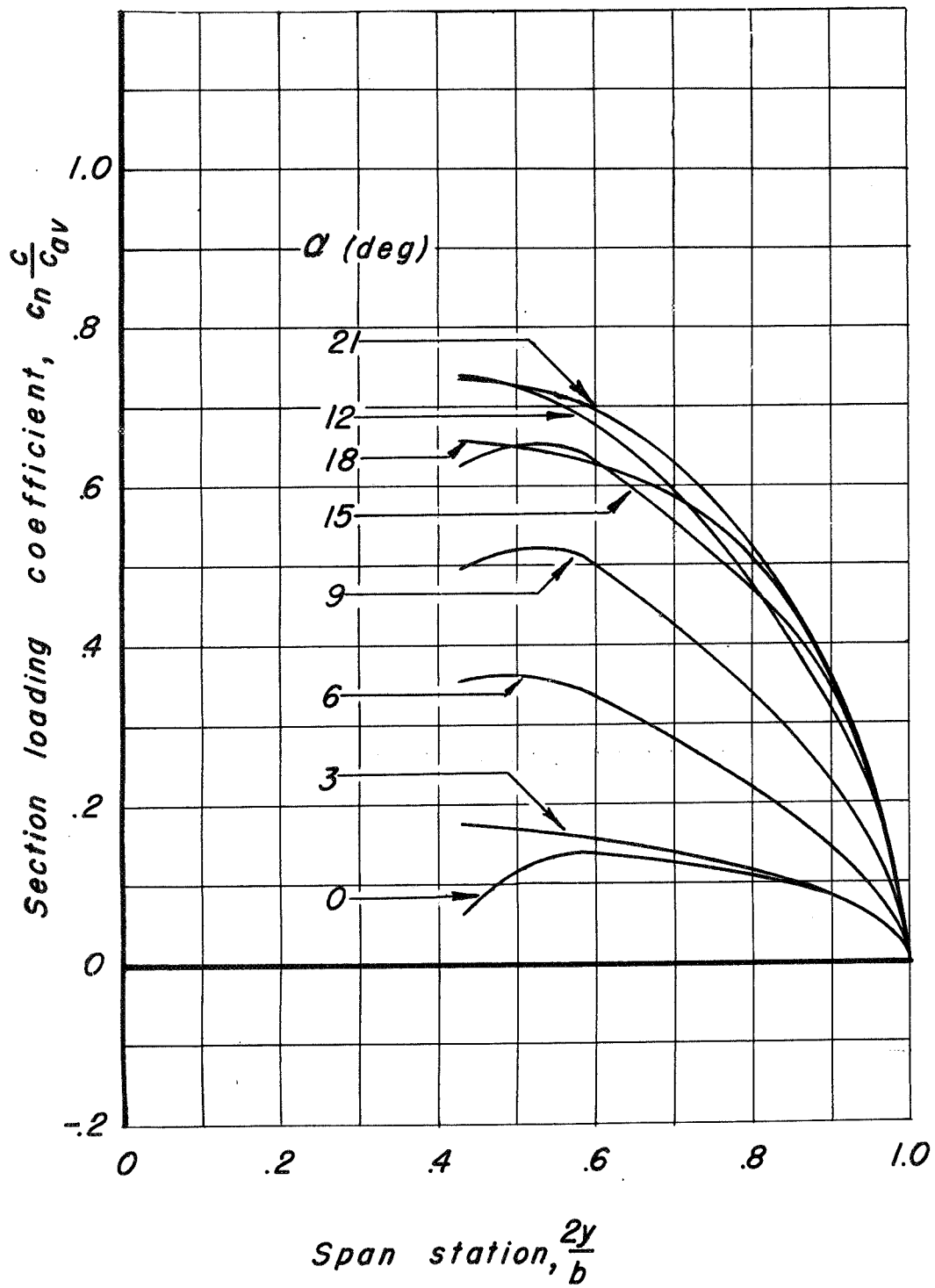

(a) Mach number, 0.40.

Figure 12.- The spanwise distribution of load on the wing of the MX-656 model. ψ, 0°; δ_{lf}, 0°.

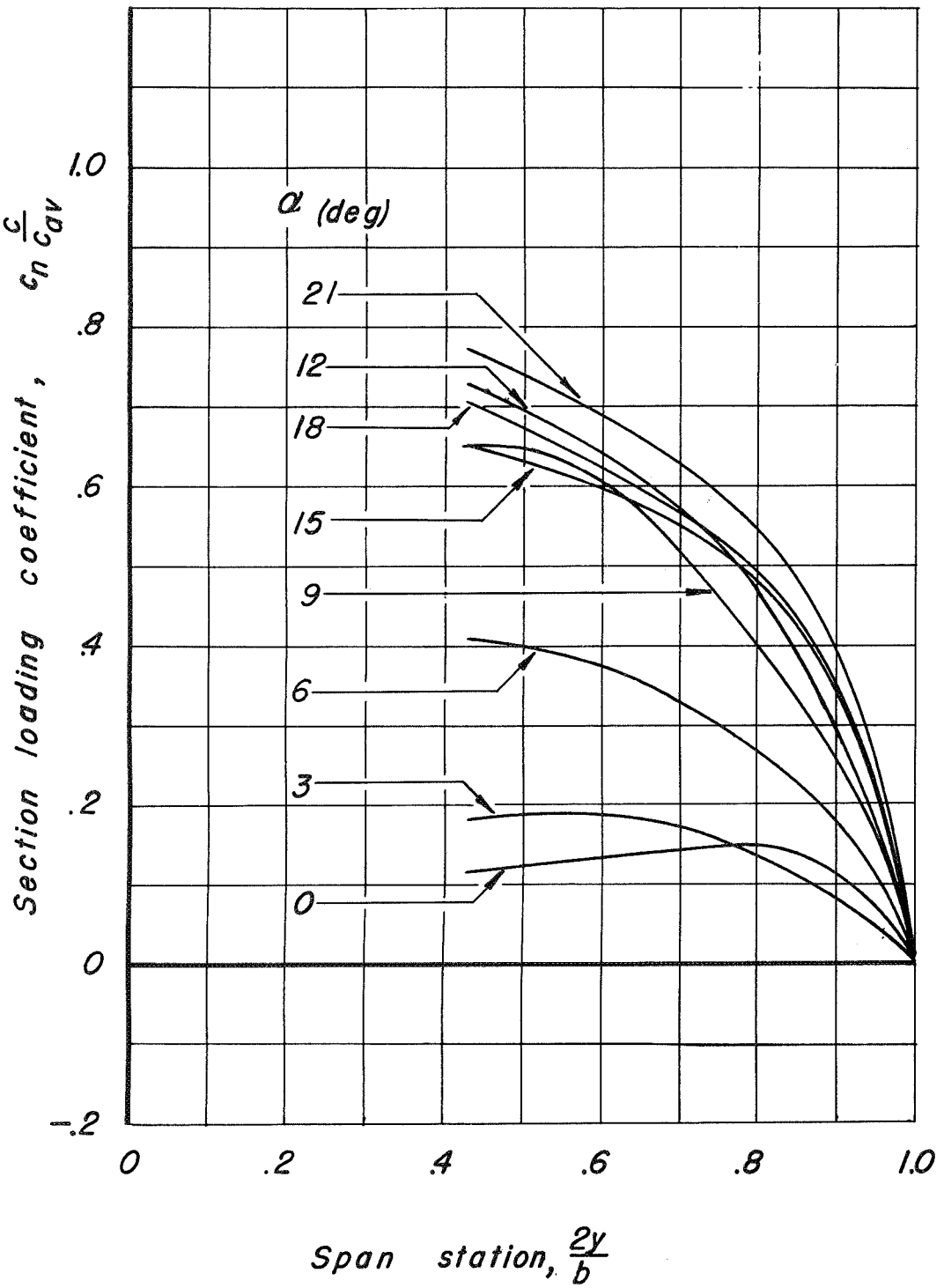

(b) Mach number, 0.60.

Figure 12.- Continued.

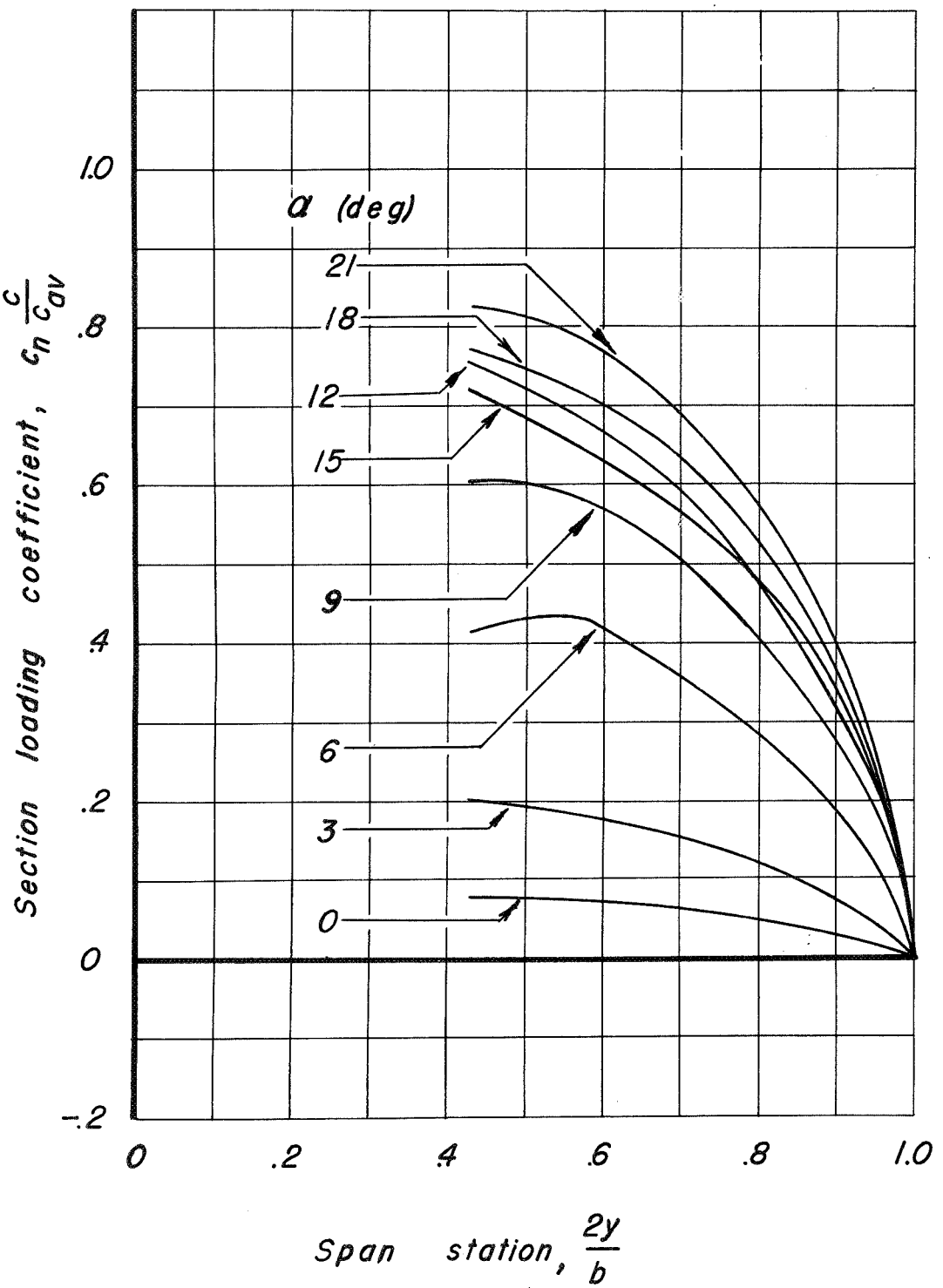

(c) Mach number, 0.80.

Figure 12.–Continued.

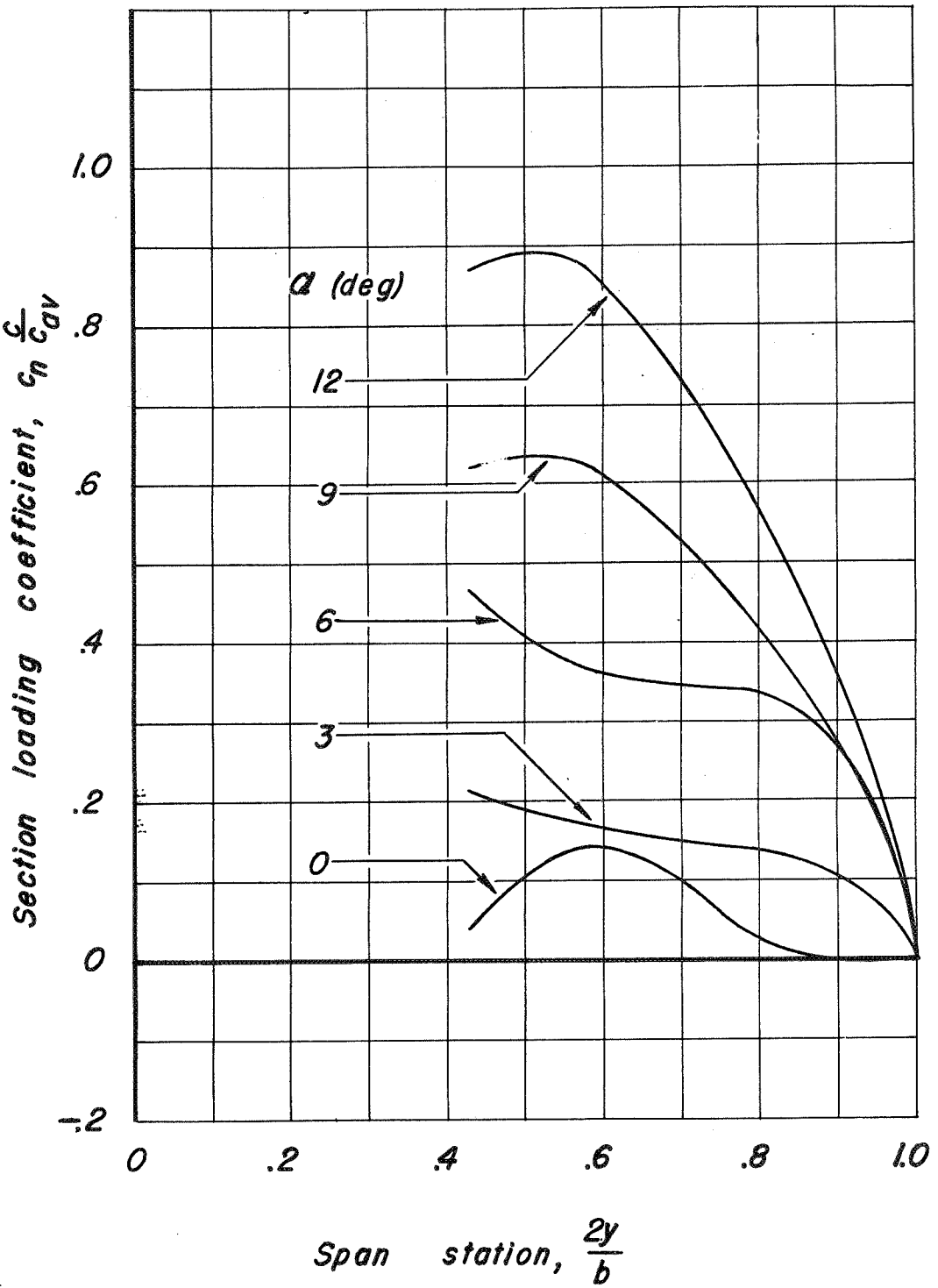

(d) Mach number, 0.90.

Figure 12.- Continued.

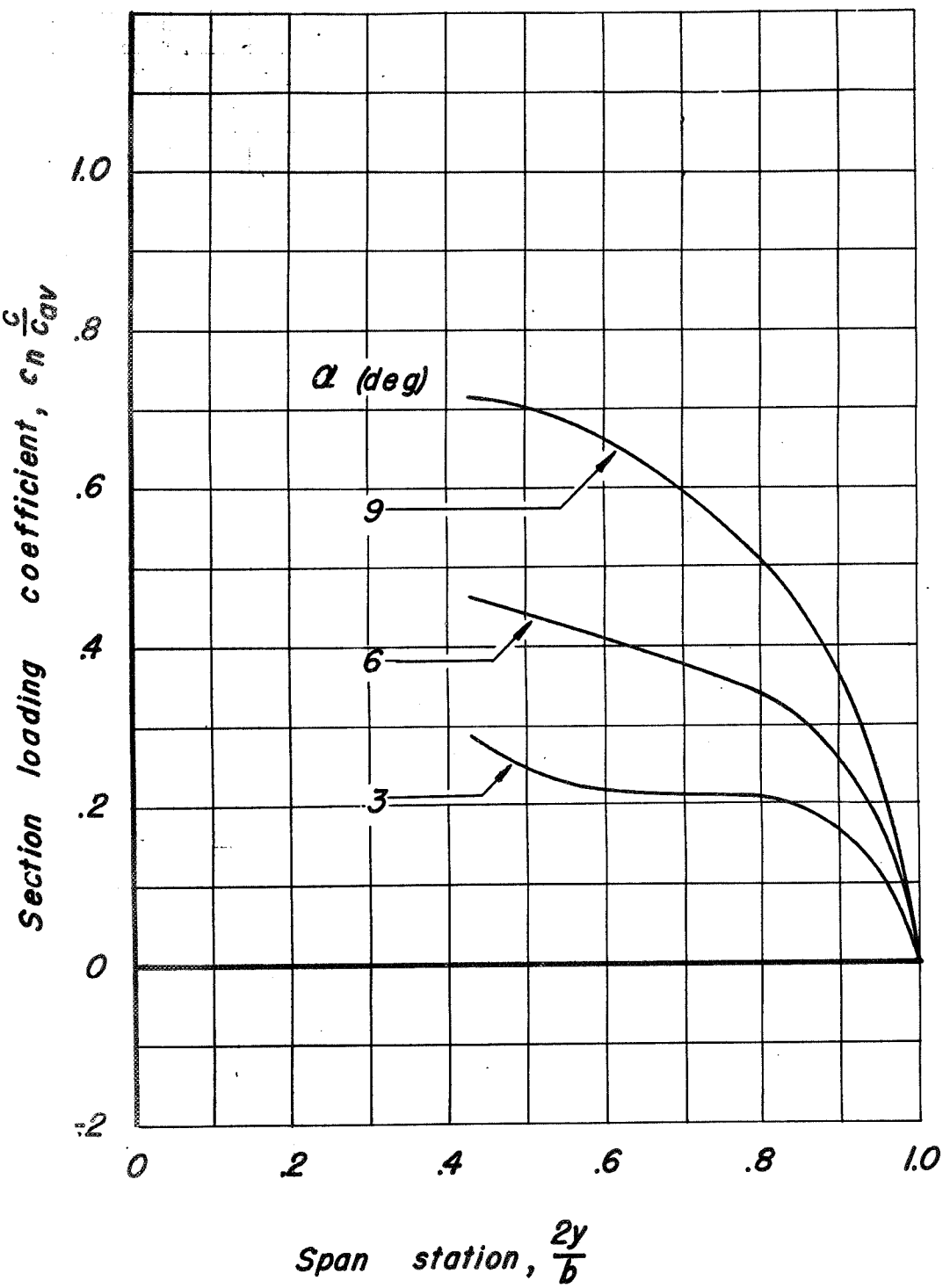

(e) Mach number, 0.925.

Figure 12.-Concluded.

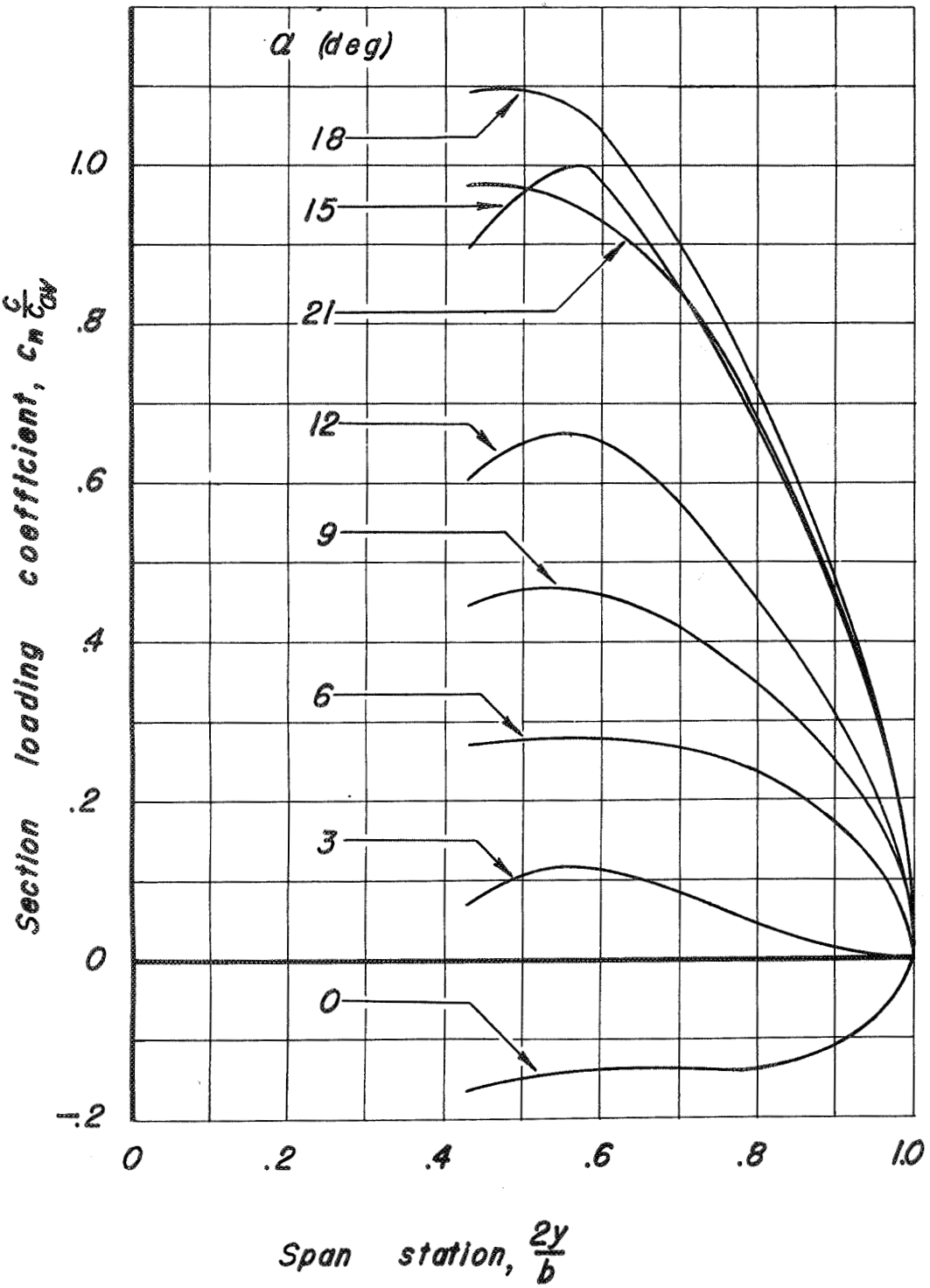

(a) Mach number, 0.40.

Figure 13.—The spanwise distribution of load on the wing of the MX-656 model. Ψ, 0°; δ_{lf}, 30°.

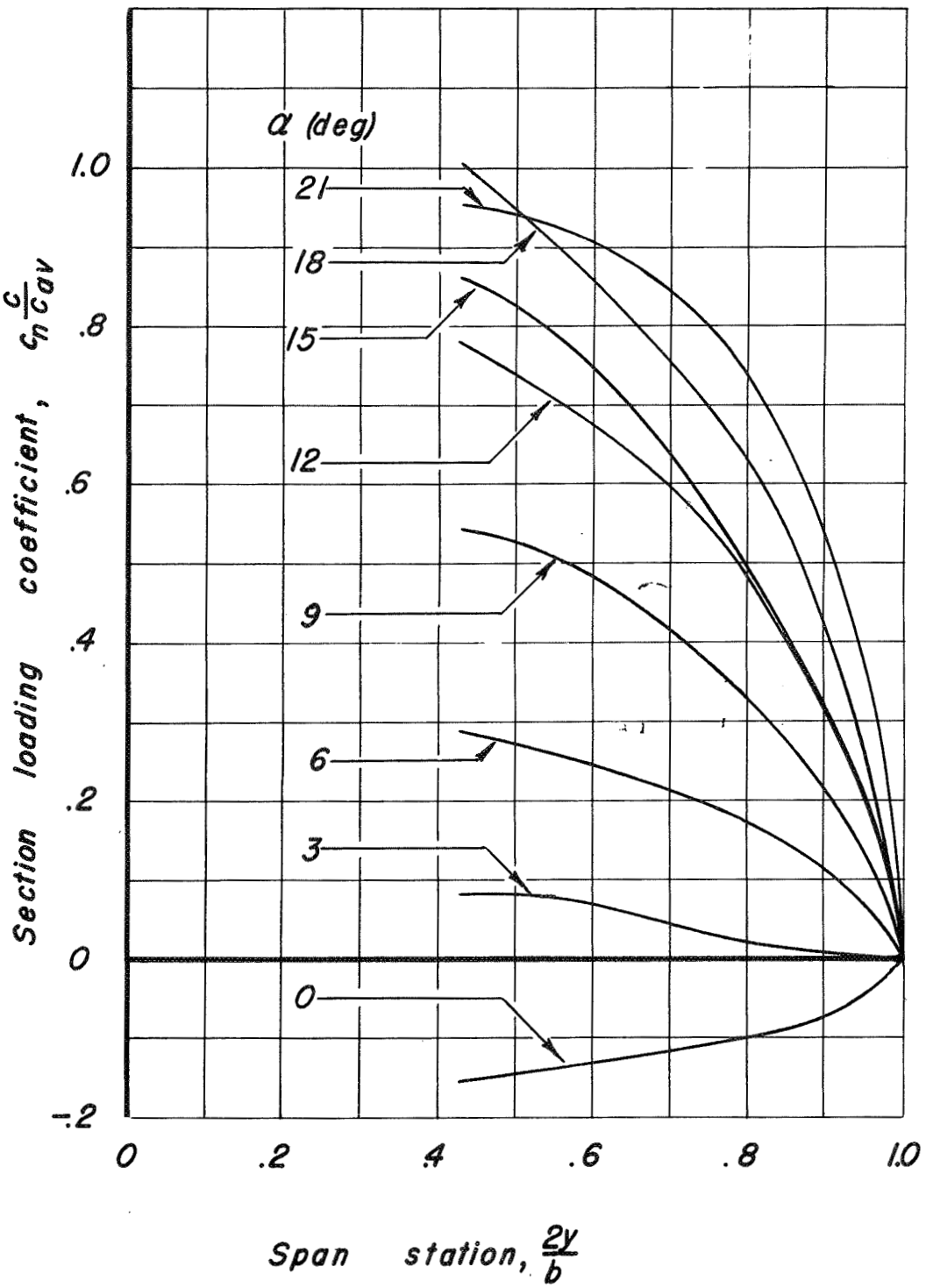

(b) Mach number, 0.60.

Figure 13.—Continued.

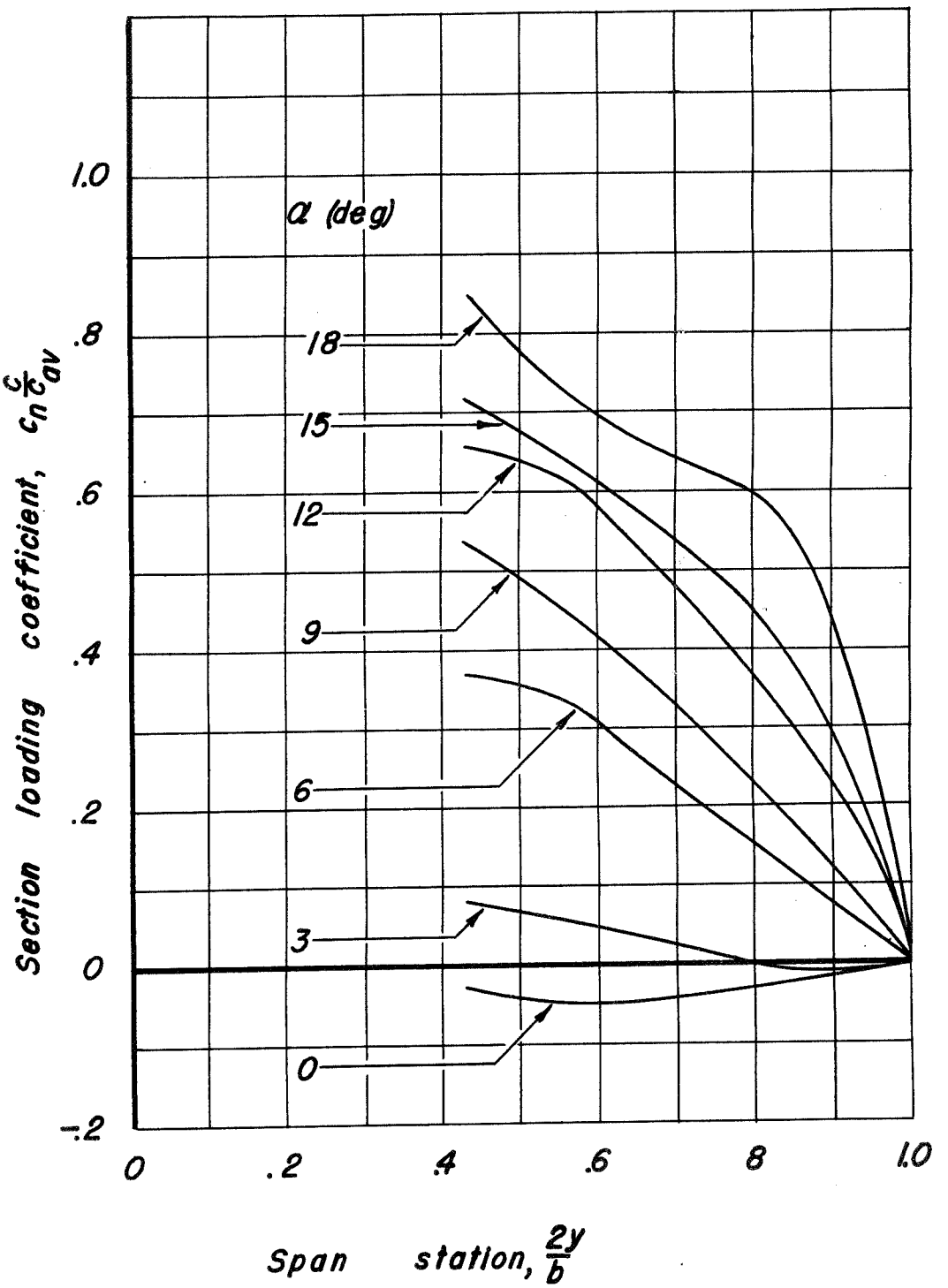

(c) Mach number, 0.80.

Figure 13.–Continued.

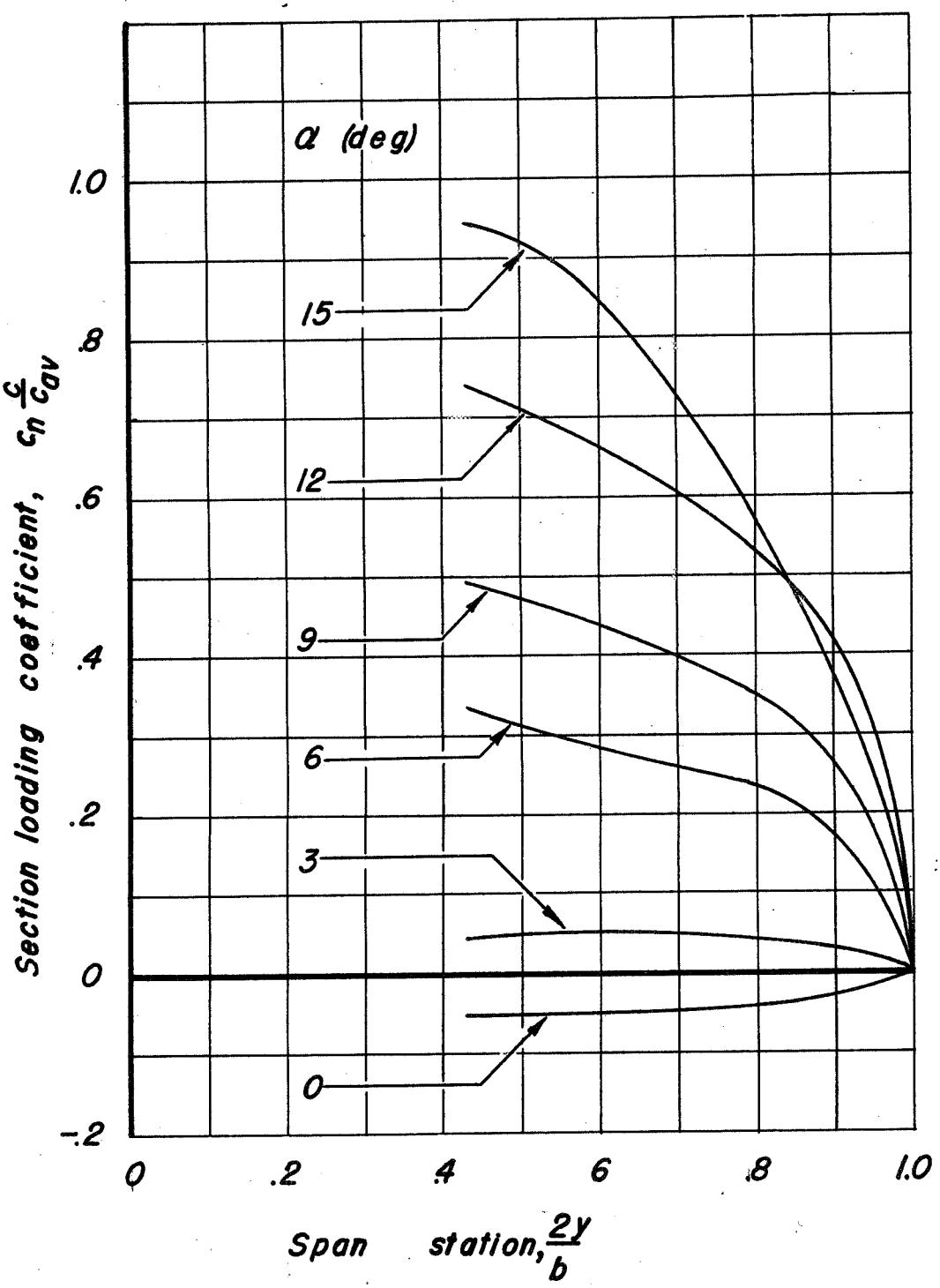

(d) Mach number, 0.90.

Figure 13.- Continued.

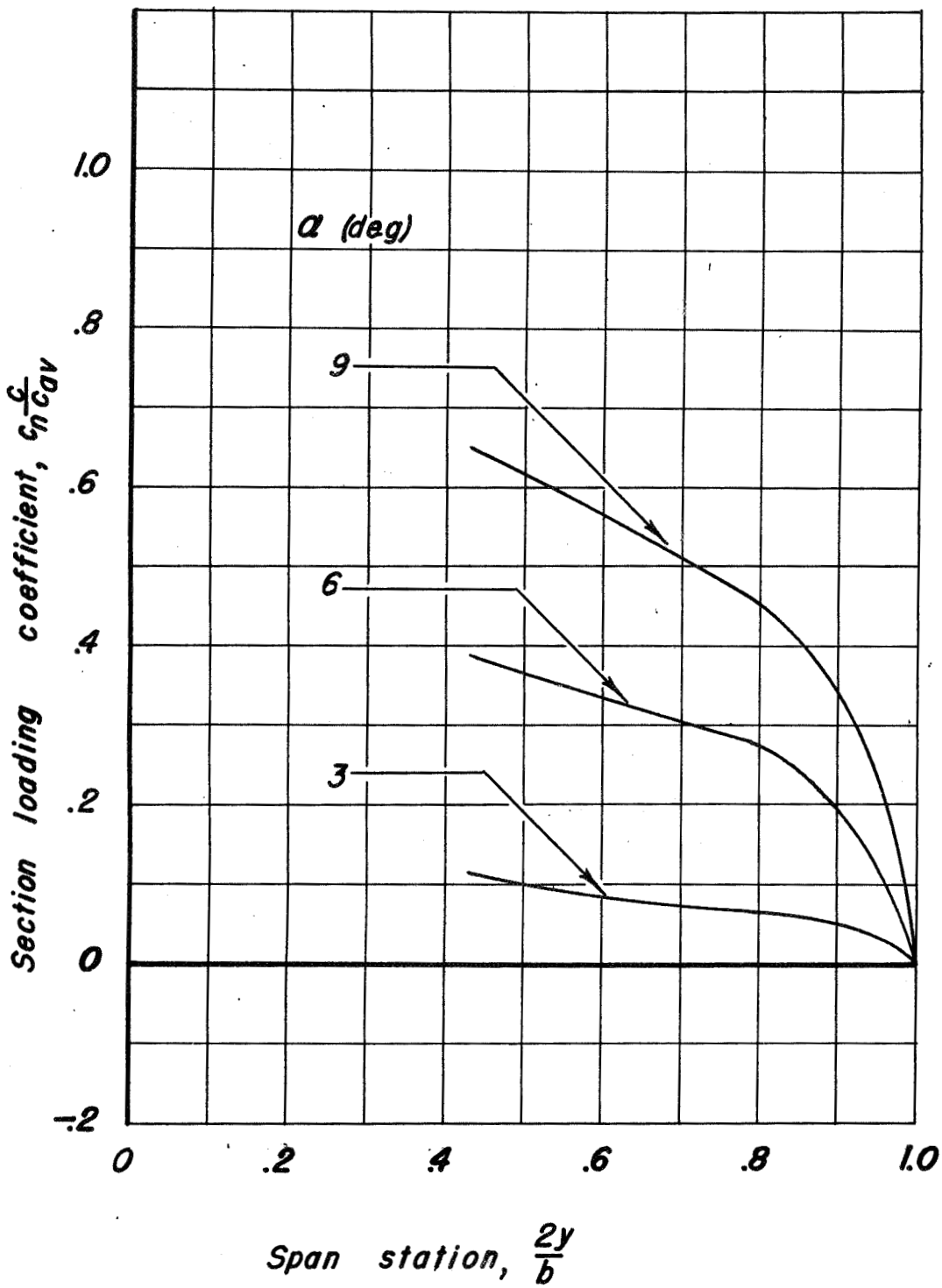

(e) Mach number, 0.925.

Figure 13.- Concluded.

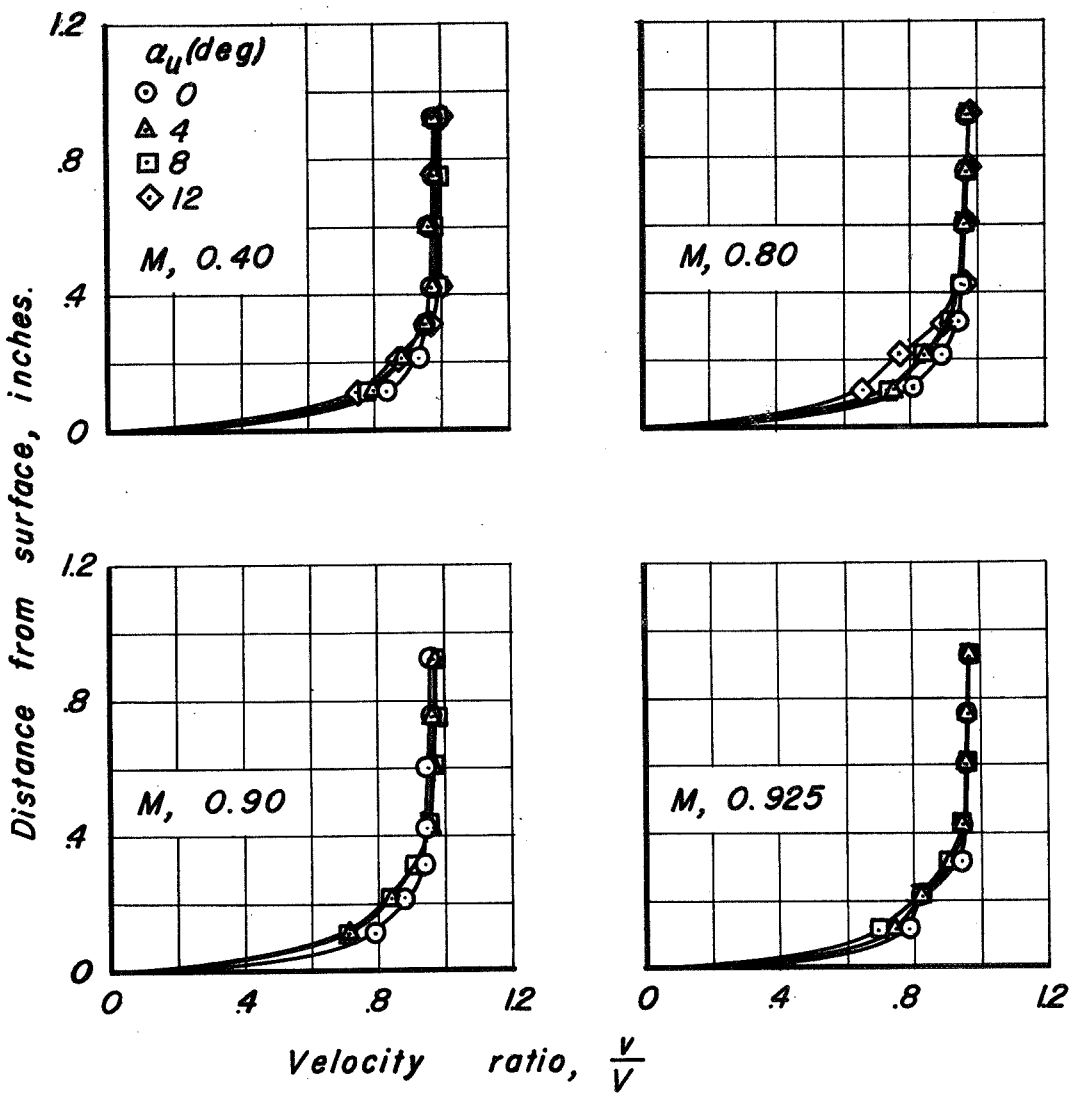

Figure 14.– The velocity ratio in the fuselage boundary layer of the MX–656 model at station 43.2 inches. ψ_u, 0°.

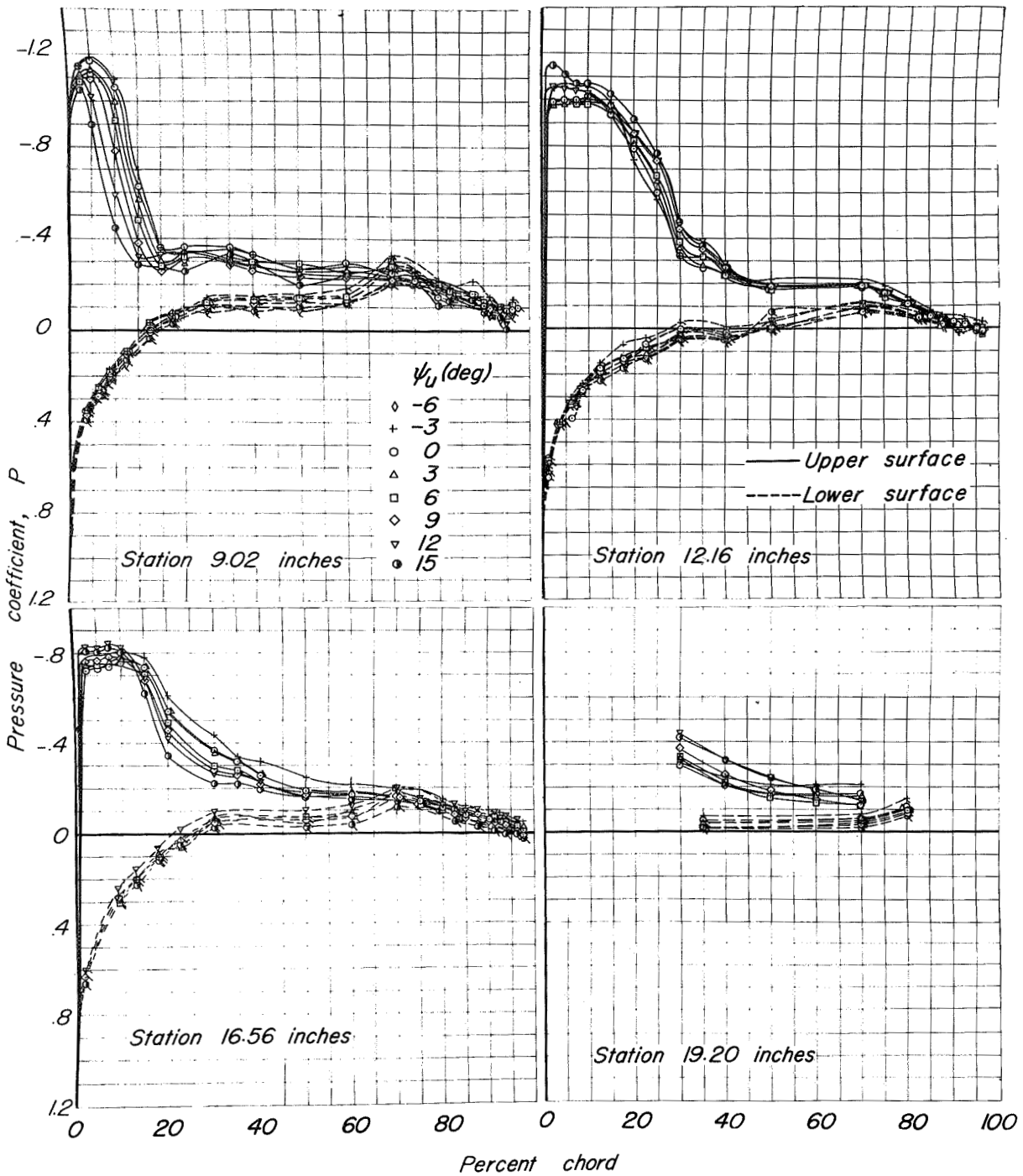

(a) Mach number, 0.40.

Figure 15.—The pressure distribution over the wing of the MX-656 model. α_u, 6.2°; δ_{lf}, 0°.

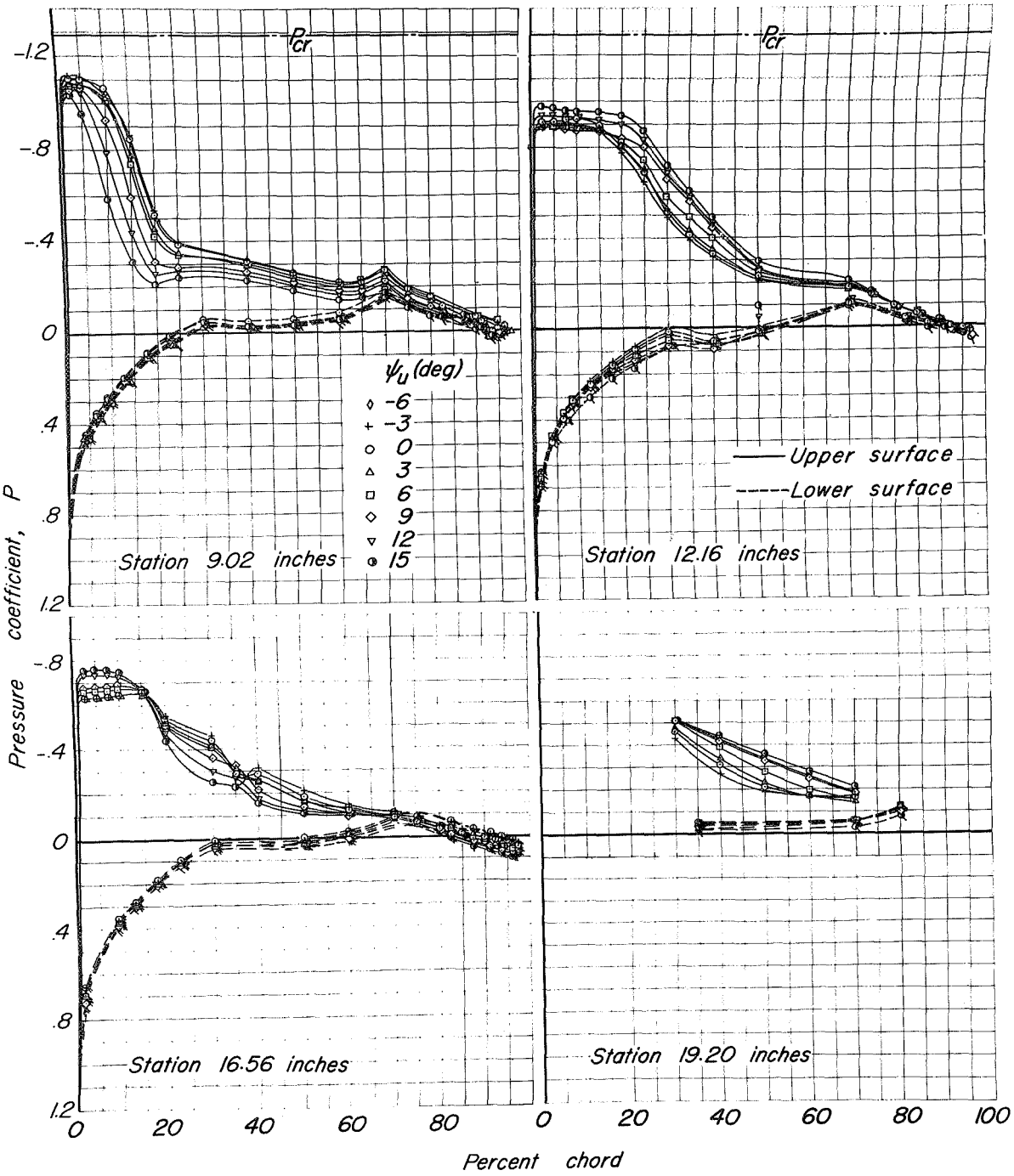

(b) Mach number, 0.60.

Figure 15.–Continued.

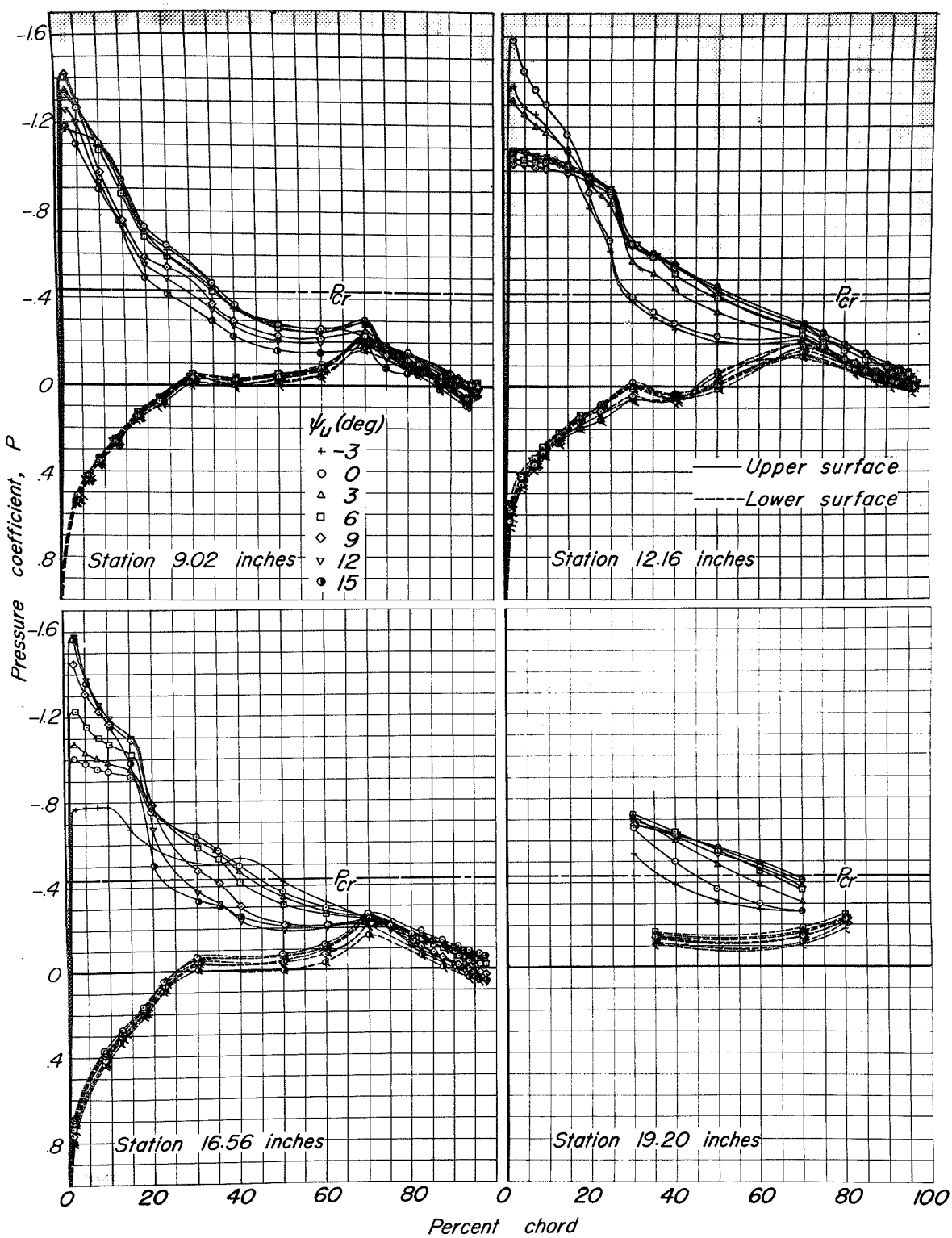

(c) Mach number 0.80.

Figure 15.–Continued.

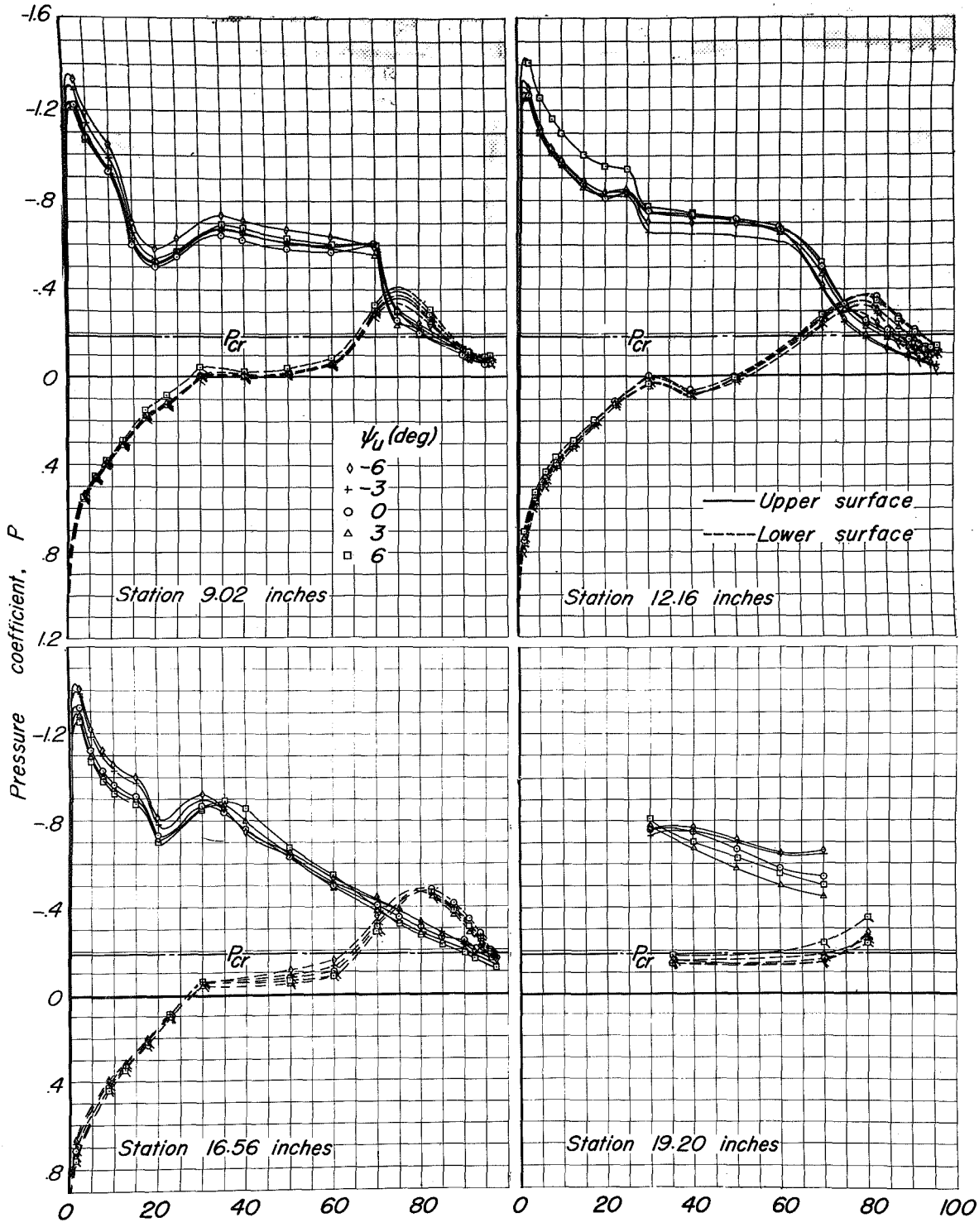

(d) Mach number, 0.90.

Figure 15.—Concluded.

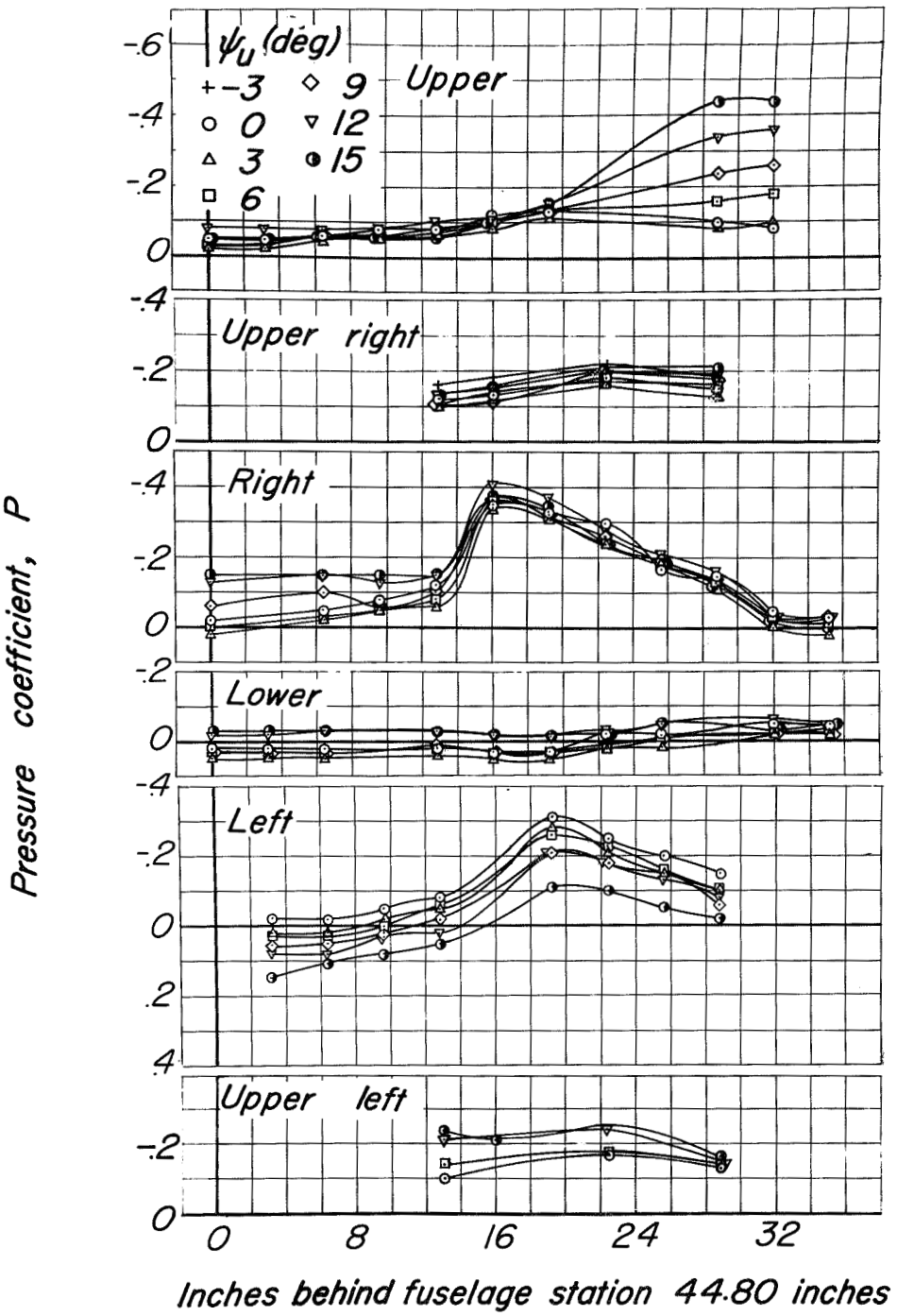

(a) Mach number, 0.40.

Figure 16.- The pressure distribution over the fuselage of the MX-656 model. α_u, 6.2°; δ_{lf}, 0°.

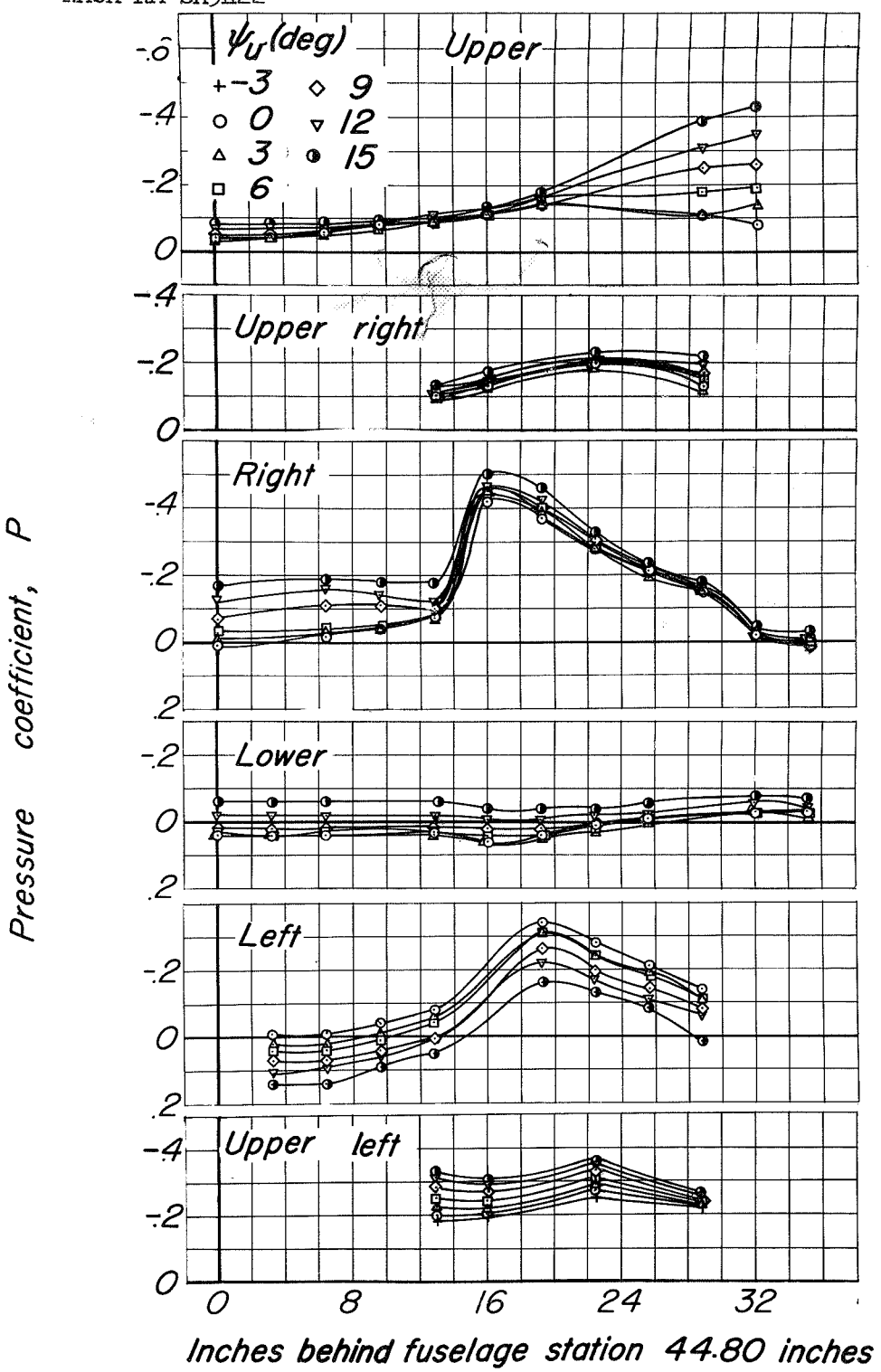

(b) Mach number, 0.60.

Figure 16.- Continued.

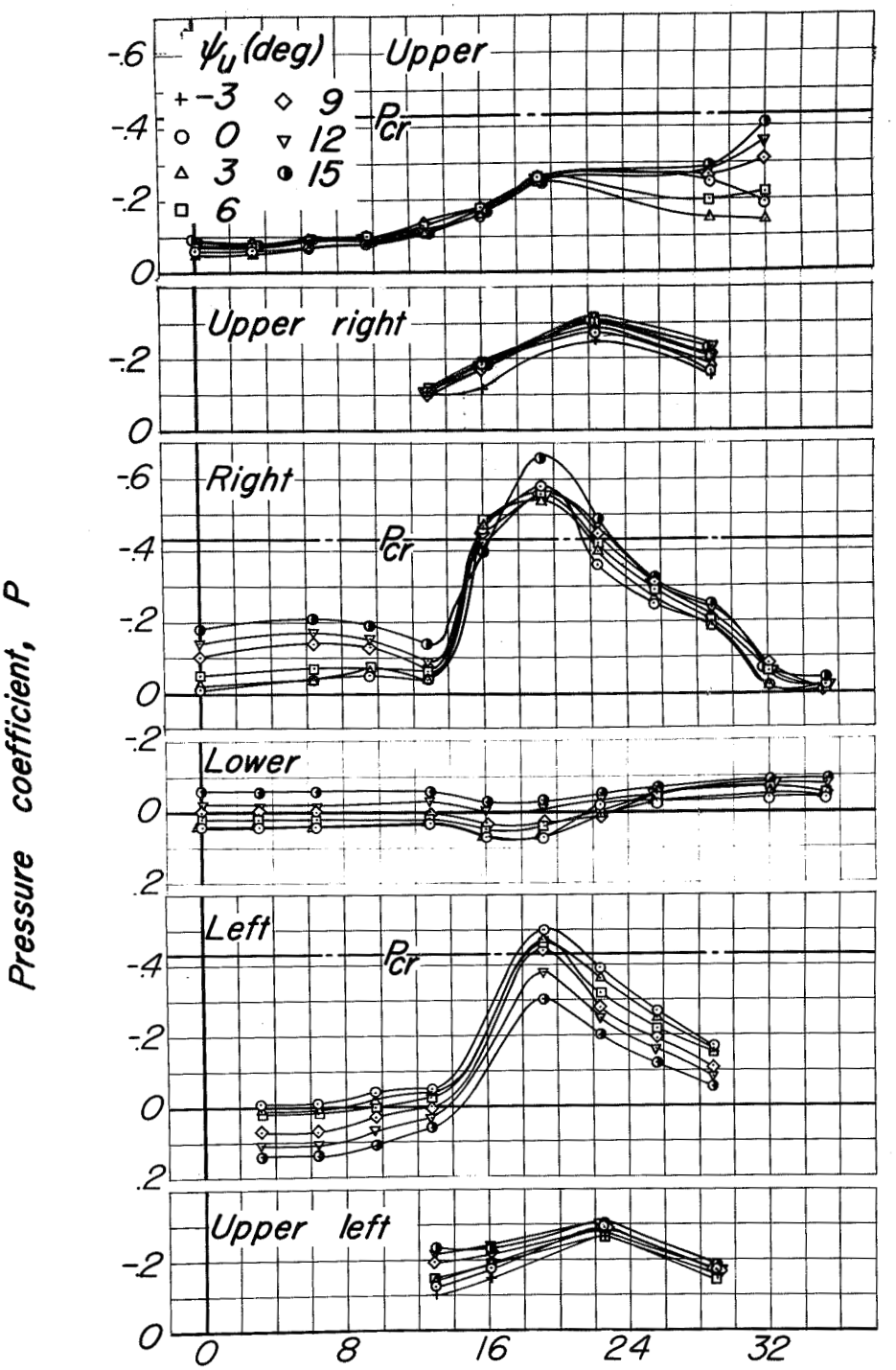

(c) Mach number 0.80.

Figure 16.—Continued.

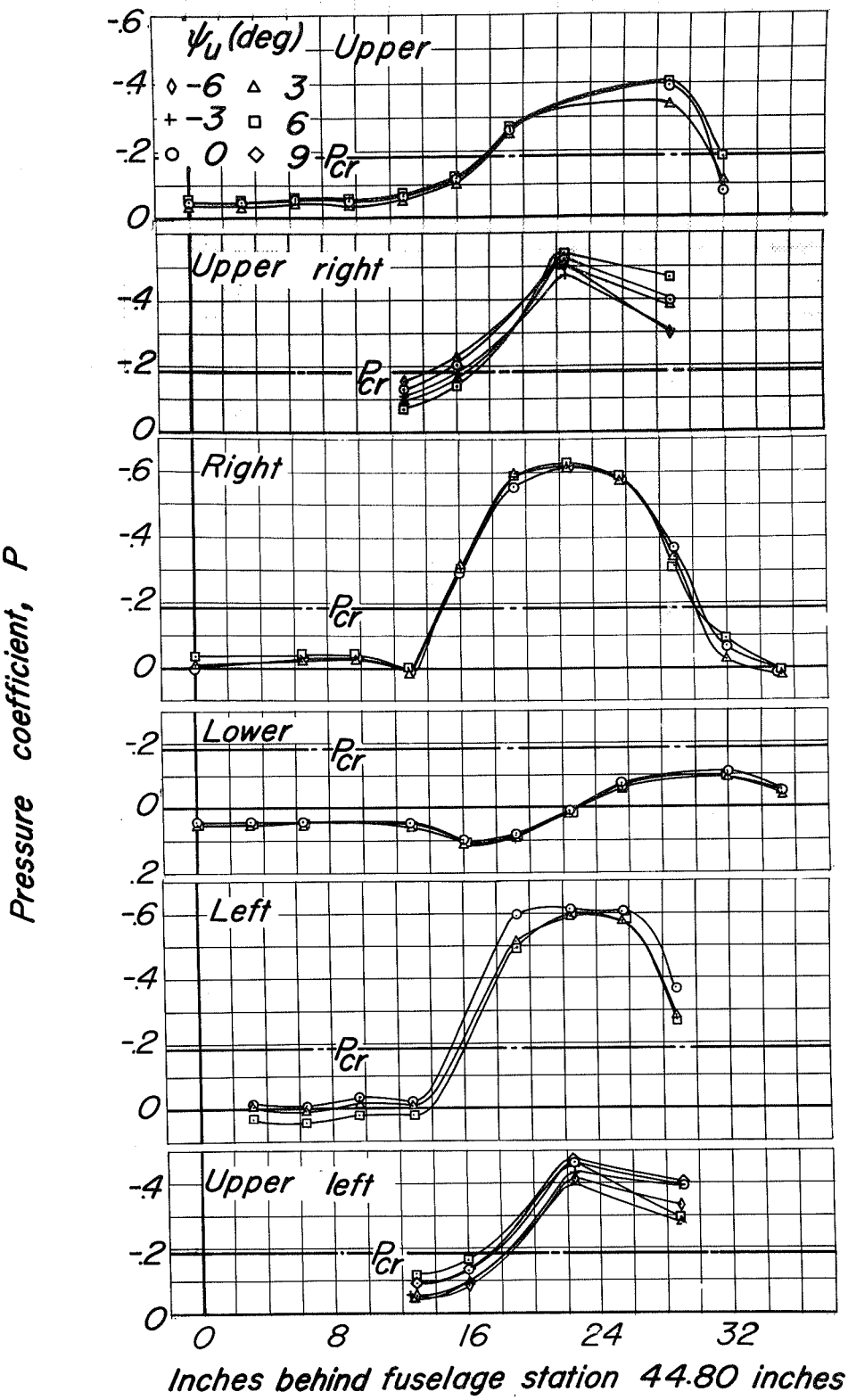

(d) Mach number, 0.90.

Figure 16.- Concluded.

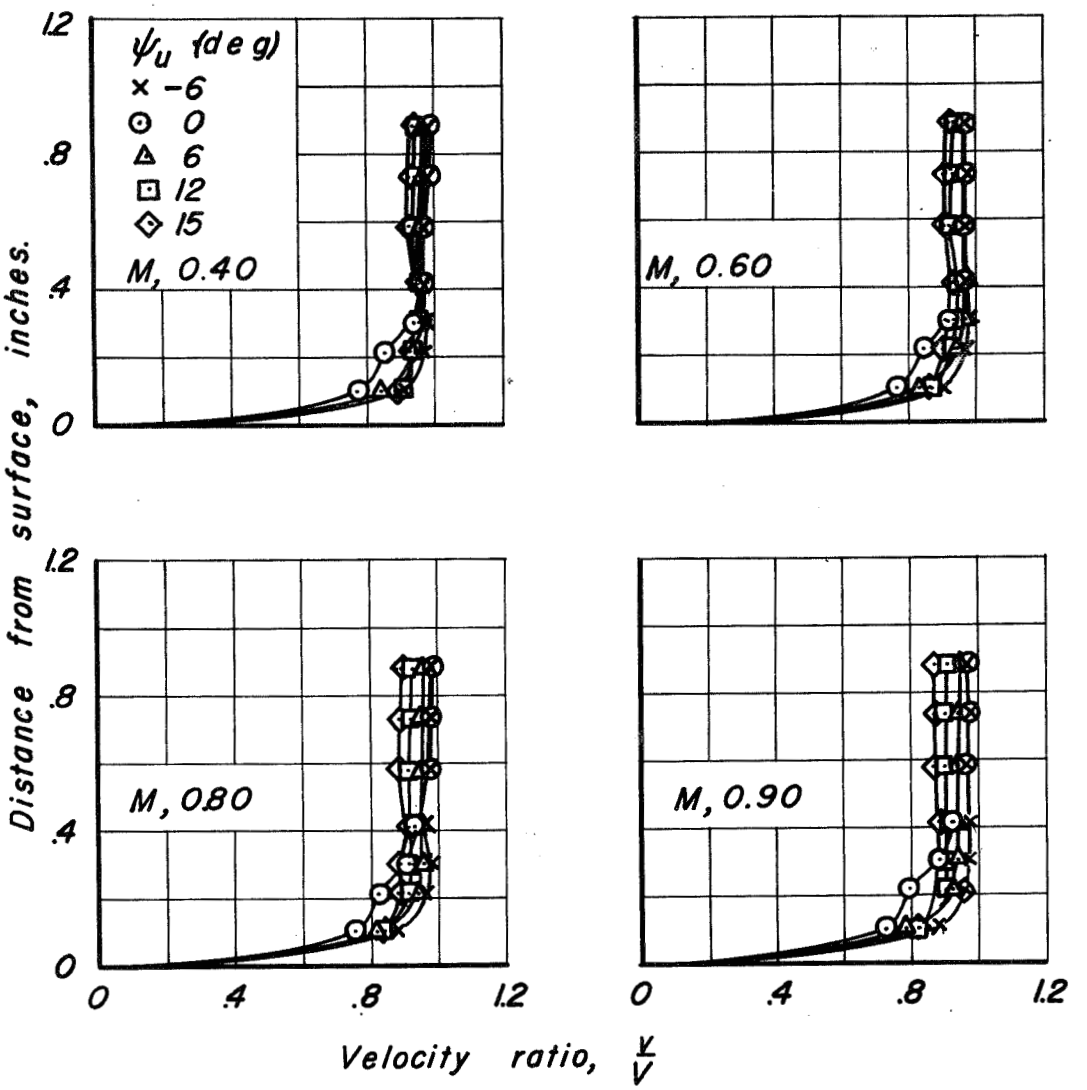

Figure 17.–The velocity ratio in the fuselage boundary layer of the MX-656 model at station 43.2 inches. α_u, 6.2°.